Deterministic Lateral Displacement for Characterization of bacterial secretion

Anastasia Syntychaki | Spring 2014

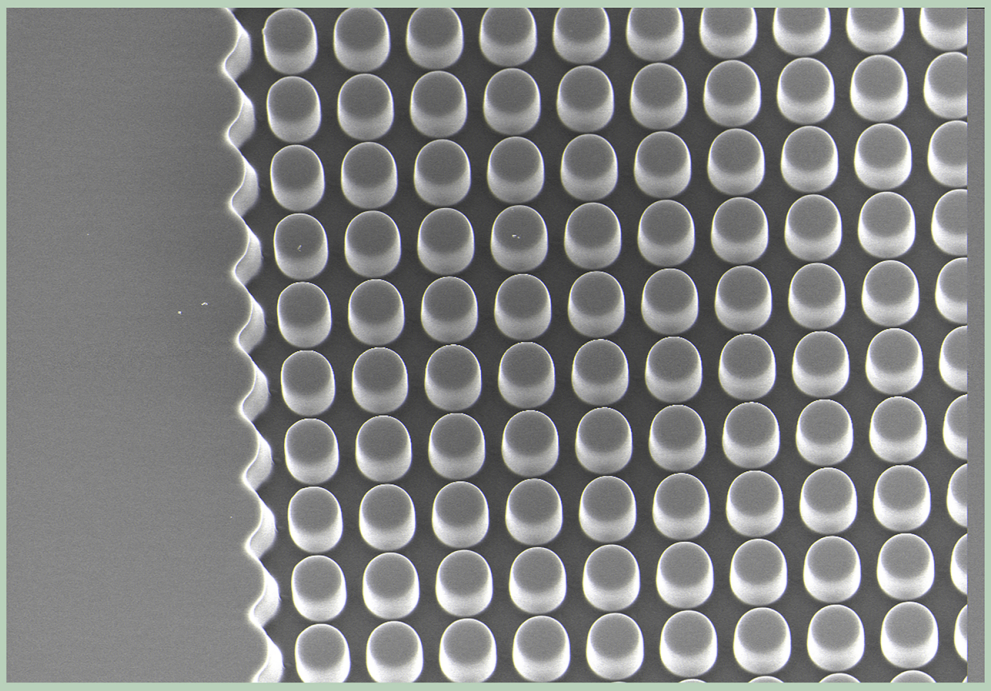

Division of Solid State Physics
Department of Physics
Lund University

Deterministic Lateral Displacement for Characterization of bacterial secretion

Master Thesis

Anastasia Syntychaki

Supervisor:
Prof. Jonas Tegenfeldt

Co-supervisors:
Stefan Holm
Dr. Jason Beech

Spring 2014

Department of Physics
Division of Solid State Physics

LUND
UNIVERSITY

Division of Solid State Physics
Department of Physics
Lund University
P.O. Box 118
SE-221 00 Lund
Sweden

Printed in Sweden by Media-Tryck, Lund University
August 2014

Abstract

In this project a new method for monitoring the bacterial secretion is presented. Knowledge on how differently cellular sub-populations behave under certain conditions can allow for the discovery of targeted medications that are specific for the active cells. The presented method is based on the deterministic lateral displacement (DLD) microfluidic technique that is used for sorting of particles according to their size, shape and mechanical properties. Particles in a DLD device interact with an array of fixed posts. Depending on the effective size of the particles, they follow different trajectories.

Pseudomonas atlantica bacteria were initially encapsulated in agarose gel droplets that functioned as biosensors, using droplet-based microfluidics. The secretion of the β-agarase enzyme by the bacteria was investigated by sorting the agarose particles in the DLD device based on their deformability. The sample was run in the DLD device using water and oil as media and the deformability results were compared. As an additional negative control, the non-secreting bacteria *Bacillus subtilis* as well as polystyrene beads were encapsulated and the droplets were examined in the DLD device for their deformability.

A tendency of the droplets that contained the secreting bacteria to soften by the secreted enzyme was observed, due to hydrolysis of the agarose gel. At high applied flow pressures the soft droplets that were run in water exhibited a high degree of deformation, thus a small effective size. On the contrary the droplets that were run in oil, the ones that contained the non-secreting bacteria as well as those with the polystyrene beads, were more rigid, thus less deformable. At lower pressures however, all samples showed a similar degree of deformation. Hence, as expected, the overall deformation of the more rigid droplets exhibited a smaller dependence on the applied pressure, compared to that of the hydrolyzed droplets in water. In the future, more experiments and positive controls as well as the extension of the method in

other systems, would be necessary for the verification of the results.

KEYWORDS: Deterministic Lateral Displacement, Secretion, Heterogeneity, Microfluidics, Lab-on-a-Chip.

Acknowledgements

First of all, I would like to thank my supervisor, Prof. Jonas Tegenfeldt for giving me the opportunity to work on such an interesting project. I am very grateful for all his help, support and continuous guidance throughout this project as well as for all our constructive discussions that helped me gain a deeper insight into the important aspects of the project.

Secondly, I would like to thank Stefan Holm, for all the time he invested on helping me overcome any obstacles that I might have encountered. I would also like to thank him for helping me with the SEM work as well as for teaching me the silanization process. Finally, I would like to thank him for our very good cooperation.

I would also like to thank Dr. Jason Beech for all his great inputs and ideas that helped me and inspired me to think outside of the box.

I would also like to express my gratitude to Dr. Claes von Wachenfeldt from the Biology Department, for providing us with the bacterial samples and for teaching me how to cultivate the *Bacillus subtilis* cells.

I also want to thank the Bio group in the Solid State Physics division for the interesting weekly meetings and for the nice working atmosphere.

Last but not least, I would like to thank my family and friends for their encouragement and their support throughout difficult times and for always being there for me.

List of Acronyms and Notations

A	Surface area
Ca	Capillary number
D	Diameter
Da	Dalton
D_{eff}	Effective diameter
d	Post gap
E	Energy
F	Force
h	Characteristic dimension
k	Spring constant
L	Length
N	DLD array periodicity
Q	Flow rate
R, r	Radius
R_s	Microfluidic resistance
Re	Reynolds number
R_{eff}	Effective radius
R_c	Critical radius

S	Ellipsoid surface
t	Time
v	Velocity
w	Width
Y	Young modulus
DLD	Deterministic lateral displacement
EPS	Extracellular polysaccharide
FACS	Fluorescence-activated cell sorting
FADS	Fluorescence-activated droplet sorting
HMP	High melting point
LB	Luria-Bertani
PBS	Phosphate buffered saline
PDMS	Polydimethylsiloxane
PEG	Polyethylene glycol
PLL	Poly-L-lysine
POC	Point-of-care
RBC	Red blood cell
SEM	Scanning electron microscopy
ULMP	Ultra low melting point
α	Parabolic flow factor
γ	Interfacial tension
$\dot{\gamma}$	Shear strain rate
$\Delta L, \Delta s$	Deformation
ΔP	Pressure difference
$\Delta\lambda$	Post row shift

ϵ	Normal strain
θ	Array angle
λ	Post center-to-center distance
μ	Fluid viscosity
ρ	Fluid density
σ	Normal stress
τ	Shear stress

Table of Contents

List of Figures

1 Introduction

In order to function, cells usually transmit certain signals by secreting proteins and other substances as well as by changing the pH and other parameters of their surrounding environment. So far there exist many studies where the cellular behaviour is examined as a bulk, meaning that a whole cellular population is observed and characterized for its function. Bulk assays are usually performed in microtiter plates or petri dishes. However several studies have demonstrated that responses to external stimuli, such as secretion, may vary within a certain cellular population (Tay *et al.*, 2010) due to, for instance, variations in the genes' expression. These findings lead to the questioning of the selectivity of existing medications such as vaccines and antibiotics. Hence, the investigation of heterogeneities in the signals transmitted by cells is of great importance as it can provide us with useful information that is required for the improvement and the future development of more targeted medications. Heterogeneity cannot be easily examined when observing the cellular behaviour as a bulk. For this reason, the need for the development of a technique that will allow for the investigation of the cellular responses at the single-cell level and for the isolation of heterogeneous cells is growing.

Microfluidics is a technology that nowadays finds many applications in biomedicine and biotechnology, as it allows us to manipulate and study single biological particles in a controlled manner. Droplet-based microfluidics have been extensively used for the encapsulation and treatment of single cells inside micrometer-sized droplets. The droplets, that function as bio-reactors, allow for the monitoring of the different cellular processes that take place as well as for the detection of the secreted substances for each individual cell.

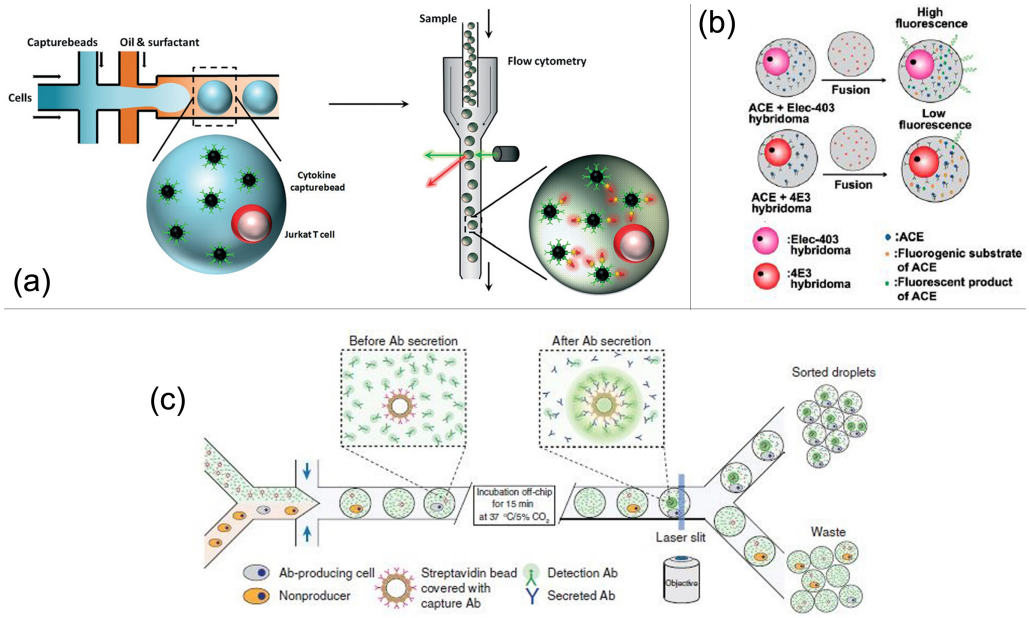

Figure 1.1: (a) T-cells are encapsulated and sorted based on the secreted cytokine using flow cytometry.[1] (b) Two types of B-cells are encapsulated and sorted based on the secreted antibodies using FADS.[2] (c) Encapsulation of hybridoma cells and optical sorting using FADS.[3]

To date there exist several studies where the secretion of single cells is investigated. For the isolation of the cells droplet-based microfluidics is used, whereas sorting of the cells based on their secretion is most commonly achieved using optical methods. In a recent work from Chokkalingam *et al.* (2013), the heterogeneity in the secretion of cytokine (IL-2, IFN-γ, TNF-α) by immune T-cells was studied. The cells were encapsulated together with cytokine capturing beads in agarose droplets using droplet-based microfluidics. The droplets were then fluorescently labelled with anti-cytokine antibodies and sorted based on the concentration of the secreted cytokine using fluorescence-activated cell sorting (FACS) (Figure 1.1a).

In another study performed by El Debs *et al.* (2012) the inhibition of an enzyme by antibodies was screened. Two different populations of hybridoma B-cells were used. The cells were encapsulated together with ACE-1 enzymes

[1] Adapted from Chokkalingam *et al.* (2013) with permission of The Royal Society of Chemistry.

[2] Reproduced from El Debs *et al.* (2012) with permission of Proceedings of the National Academy of Sciences.

[3] Adapted by permission from Macmillan Publishers Ltd: Mazutis *et al.* (2013).

in aqueous droplets in order to detect the secretion of 4E3 antibodies that are specific for the enzymes. Fluorogenic ACE-1 substrate was then added to the droplets which were sorted using fluorescence-activated droplet sorting (FADS) (Figure 1.1b).

In a similar study presented by Mazutis *et al.* (2013) mouse hybridoma cells were sorted based on their heterogeneity in the secretion of IgG antibodies. For this purpose, a microfluidics system was developed and used. The cells were encapsulated into aqueous droplets together with a fluorescent marker and beads coated with anti-IgG antibodies. Secretion of the analyte resulted in a transmission of a signal and the drops were sorted using FADS (Figure 1.1c).

Baret *et al.* (2009) presented a study where mixed populations of two different types of E. coli bacteria were initially encapsulated in droplets. The droplets were then fused with a fluorogenic β-galactosidase substrate. The substrate was hydrolyzed by the secreted β-galactosidase enzyme, in case that the latter was present. Hydrolysis of the substrate gives a fluorescent product and the droplets containing the bacteria are sorted using FADS.

Finally, in an early study presented by Powell and Weaver (1990) the secretion of antibodies by mouse hybridoma cells was investigated. Hybridoma cells were encapsulated into agarose droplets together with anti-mouse antibodies for capturing. Non-secreting masticytoma cells were separately encapsulated as a negative control. All droplets were then fluorescently labelled. Flow cytometry was used for sorting based on the fluorescent signal that corresponded to the amount of the secreted molecules.

Nevertheless, sorting based on the particles' fluorescent properties is complicated as it requires the co-encapsulation of capturing beads and some kind of labeling with fluorescent markers or substrates. In addition the use of flow cytometry equipment is needed. Flow cytometry is a reliable sorting method but it has several drawbacks: it consists of expensive, non-portable equipment that is complex and not always easy to handle.

In the current project a label-free method for the isolation of bacterial cells based on their secretion is presented. Sorting is achieved based on the mechanical properties of droplets that contain the secreting bacteria. *Pseudomonas atlantica* bacteria are used as a model system and are sorted based on their secretion of β-agarase enzymes. The cells are initially encapsulated in agarose gel droplets using droplet-based microfluidics. Beta-agarase is known for its ability to hydrolyze the agarose, the enzyme's substrate. Thus, the secreted β-agarase from the encapsulated bacteria will hydrolyze the agarose droplets, resulting in their softening. The bacteria-containing

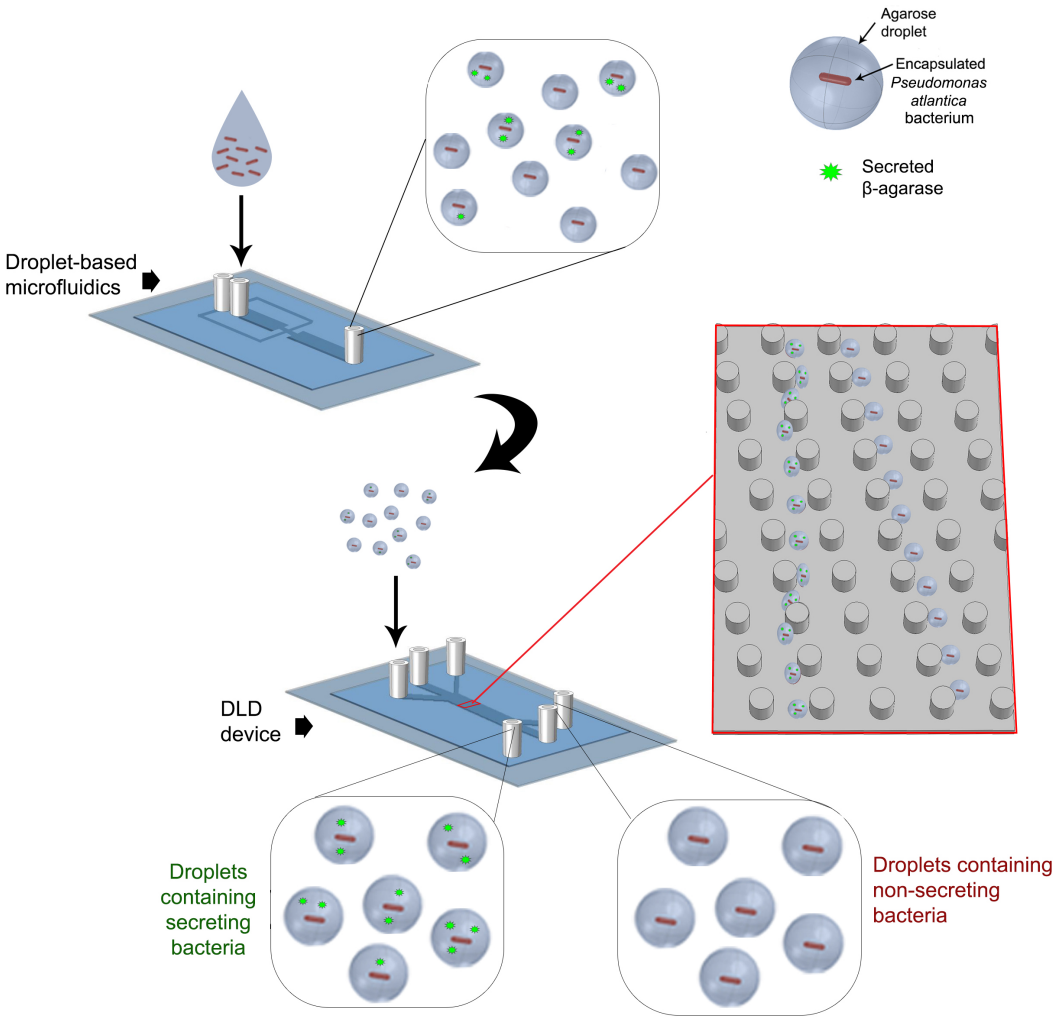

Figure 1.2: Schematic overview of the method presented in this project for sorting bacteria based on their secretion of β-agarase. *Pseudomonas atlantica* bacteria are initially encapsulated into agarose droplets. During the incubation of the droplets, the bacteria secrete β-agarase enzymes that hydrolyze the agarose gel. The droplets are then sorted based on their deformability using a deterministic lateral displacement (DLD) device.

droplets are then sorted in a Deterministic Lateral Displacement device (DLD), introduced by Huang *et al.* (2004), based on their deformability. The DLD is a cheap, easy-to-handle microfluidic device allowing for continuous sorting of biological samples based on their size, shape and deformability. The function of the DLD method is based on the steric interactions of the particles with fixed posts in the device and can suit several applications. The principle of its operation is analytically described in Chapter 3. Figure 1.2 illustrates the method presented for the detection of β-agarase.

This thesis is divided into 9 chapters. Initially the basics of the microfluidics theory are given in Chapter 2. Chapter 3 presents the principle of operation of the Deterministic Lateral Displacement method for the separation of particles. In addition deformation of particles is discussed. Chapter 4 deals with droplet-based microfluidics and its application for particle synthesis and particle encapsulation. In addition the droplet-based device designs are presented. Chapter 5 gives a general overview of hydrogels and their characteristics. Furthermore, the properties of agarose gels used in the current work are described. In Chapter 6 the basic functions of bacteria are initially described. Thereafter, details on the characteristics of *Pseudomonas atlantica* bacteria are given. Chapter 7 discusses the experimental methodology used for the encapsulation of bacteria in polymeric droplets and for their isolation using the DLD method. In Chapter 8 the quantified results of the experiments for the bacterial encapsulation and for the characterization of the droplets are presented and discussed. Finally, in Chapter 9 the main conclusions of the thesis are summarized and an outlook for future improvements and applications is presented.

References

Baret, J.-C., Miller, O. J., Taly, V., Ryckelynck, M., El-Harrak, A., Frenz, L., Rick, C., Samuels, M. L., Hutchison, J. B., Agresti, J. J., Link, D. R., Weitz, D. A., and Griffiths, A. D. (2009), Fluorescence-activated droplet sorting (FADS): efficient microfluidic cell sorting based on enzymatic activity, *Lab Chip* 9 (13), pp. 1850–1858, DOI: 10.1039/b902504a.

Chokkalingam, V., Tel, J., Wimmers, F., Liu, X., Semenov, S., Thiele, J., Figdorb, C. G., and Huck, W. T. S. (2013), Probing cellular heterogeneity in cytokine-secreting immune cells using droplet-based microfluidics, *Lab Chip* 13 (24), pp. 4740–4744, DOI: 10.1039/c3lc50945a.

El Debs, B., Utharala, R., Balyasnikova, I. V., Griffiths, A. D., and Merten, C. A. (2012), Functional single-cell hybridoma screening using droplet-based microfluidics, *PNAS* 109 (29), pp. 11570–11575, DOI: 10.1073/pnas.1204514109.

Huang, L. R., Cox, E. C., Austin, R. H., and Sturm, J. C. (2004), Continuous Particle Separation Through Deterministic Lateral Displacement, *Science* 304 (5673), pp. 987–990, DOI: 10.1126/science.1094567.

Mazutis, L., Gilbert, J., Ung, W. L., Weitz, D. A., Griffiths, A. D., and Heyman, J. A. (2013), Single-cell analysis and sorting using droplet-based microfluidics, *Nature Protocols* 8 (5), pp. 870–891, DOI: 10.1038/nprot.2013.046.

Powell, K. T. and Weaver, J. C. (1990), Gel Microdroplets and Flow Cytometry: Rapid Determination of Antibody Secretion by Individual Cells Within a Cell Population, *Nature Biotechnology* 8 (4), pp. 333–337, DOI: 10.1038/nbt0490-333.

Tay, S., Hughey, J. J., Lee, T. K., Lipniacki, T., Quake, S. R., and Covert, M. W. (2010), Single-cell NF-κB dynamics reveal digital activation and analogue information processing, *Nature* 466 (7303), pp. 267–271, DOI: 10.1038/nature09145.

2 Microfluidics theory

2.1 Introduction

Microfluidics in general is the field that deals with the behaviour of fluids at the microscale "under the action of external forces" (Bruus, 2008). For the investigation of their behaviour, fluids of volumes in the range of μL down to nL or pL are manipulated in miniaturized devices also known as lab-on-a-chip systems. Such systems enable experiments for biomedical and biotechnological applications where usually samples and reagents of small volumes are tested. The device miniaturization also allows their incorporation to point-of-care (POC) products. They are easy-to-handle systems that enable the performance of high-throughput and less costly assays.

2.2 Flow conditions

Flow at the microscale differs significantly from the flow at the macroscale. The decrease in the dimensions gives rise to new behaviours and new effects that dominate the flow. In fluidics, Newton's second law can be written as (Bruus, 2008):

$$ma = \sum_i f_i \Rightarrow \rho\left[\frac{\partial \boldsymbol{v}}{\partial t} + (\boldsymbol{v}\cdot\nabla)\,\boldsymbol{v}\right] = -\nabla p + \mu\nabla^2\boldsymbol{v} \tag{2.1}$$

also known as Navier-Stokes equation, where the term to the left corresponds to the inertial forces and the term to the right to the viscous forces. It is usually approximated that the non-linear part of the inertial term $(\overline{v}\cdot\nabla)\,\overline{v}$ is negligible and that the viscous forces dominate. The ratio between the inertial and the viscous forces is then given by the so-called Reynolds number (Re), a dimensionless number that is defined as:

$$Re = \frac{F_{inertial}}{F_{viscous}} = \frac{\rho v h}{\mu} \tag{2.2}$$

where v is the fluid velocity, h is the characteristic dimension, ρ is the fluid density and μ is the fluid viscosity. Re can thus give a measure of which term dominates the fluid flow. For high Reynolds numbers ($Re > 2000$) the inertial terms are dominant whereas a low Reynolds number ($Re < 500$) indicates the predominance of viscous forces. Flow at high Reynolds numbers is known as turbulent and is characterized by its chaotic motion, while laminar flow is dominant at lower Reynolds numbers. The high viscous forces in laminar flow are responsible for preventing co-flowing streams from mixing. Fluids at the micro- and nanoscale are dominated by laminar flow, a fact that determines their behaviour and differentiates it from that of fluids at the macroscale.

2.3 Fluid in a microchannel

The flow of a fluid in a microchannel can be driven by several means, such as pressure, capillary action and electroosmosis. Depending on the driving force, the flow profile of the fluid in the channel varies. In electroosmotically driven flow for instance the fluid has a plug-like flow profile, whereas in pressure driven flow fluids exhibit a parabolic flow profile. In that case, due to boundary conditions in the channel ("no-slip" conditions), fluid particles close to the channel wall travel slower than particles at the center of the channel where the velocity reaches its maximum. The flow rate (Q) in a microchannel is given by the expression:

$$Q = \frac{\Delta P}{R_s} \tag{2.3}$$

where ΔP is the pressure difference across the channel and R_s is the microfluidic resistance in the channel. Transition from the macroscale to smaller scales makes "pushing" of fluids inside a channel more difficult. This is a result of an increase in R_s, as implied from the expression for a rectangular channel:

$$R_s = \frac{12\mu L}{w h^3} \tag{2.4}$$

where w is the channel width and h its height.

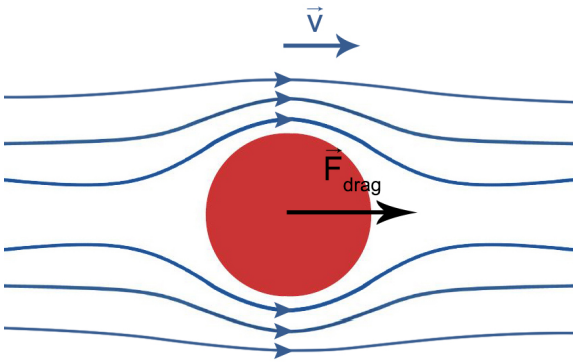

Figure 2.1: Illustration of a particle suspended in a fluid.

2.4 Particles in a fluid

A spherical particle of radius r that is suspended in a fluid will be dragged by the fluid that flows with speed $\boldsymbol{v}$ relative to the particle and will then move with the same speed (Figure 2.1). If no other external force is applied on the particle, the only force it will experience will be a viscous drag given by Stoke's equation:

$$\boldsymbol{F_{drag}} = 6\pi \boldsymbol{v} \mu r \tag{2.5}$$

However, application of additional forces on particles may alter their flowing conditions. Such forces include diffusion, which is always present, but also other externally applied forces such as steric, electrical or magnetic ones (Beech, 2011). These forces can displace the particles inside the fluid and force them to move into other streamlines, an effect that can be useful for several applications such as for particle separation. Particle separation due to steric forces will be further discussed in section 3.2

2.5 Droplet generation

One sub-category of microfluidics is droplet-based microfluidics, an increasingly growing field that is finding several applications in drug delivery and discovery, point-of-care diagnostics as well as in biomedical screening (Teh *et al.*, 2008). Such microfluidic systems are designed to form droplets by the co- or cross- flow of two immiscible liquids under laminar flow conditions.

A liquid that flows in a channel will experience shear forces by the cross-

flow of a second immiscible liquid (Streets and Huang, 2014). This will in turn result in the deformation and the destabilization of their interfaces. Such interfacial effects between immiscible phases are stronger at the microscale due to the high surface-to-volume ratio as compared to that at the macroscale (Teh *et al.*, 2008). The interfacial effects will therefore determine the droplet generation.

The liquid from which droplets are formed is known as discrete phase whereas the second immiscible liquid is the so called continuous phase. The break-up of the discrete phase to droplets is a process that depends on several parameters, such as the device geometry, the applied pressures, the viscosity of the two phases as well as the interfacial tension between them (Teh *et al.*, 2008). During the cross-flowing of the two phases, the interfacial tension will tend to minimize their interface whereas the viscous forces will tend to extend it. The capillary pressure drop across the interface is given by the expression:

$$\Delta P_c = \gamma / r \tag{2.6}$$

where γ is the interfacial tension and r is the radius of the fluid cylinder (Holtzman *et al.*, 2012). The viscous pressure drop on the contrary is given by the expression:

$$\Delta P_v = \mu v / h \tag{2.7}$$

where μ is the fluid viscosity, v is the characteristic fluid velocity and h is the channel width. By balancing these two pressure differences we obtain the dimensionless Capillary number (Ca),

$$Ca = \frac{viscous}{interfacial} = \frac{\mu v}{\gamma} = \frac{h}{r} \tag{2.8}$$

The dominant force is determined by the Capillary number. Above a critical value for the capillary number, viscous forces dominate and droplet break-off occurs.

According to the Plateau-Rayleigh capillary instability theory, the interfacial and viscous pressure differences along the interface of the two immiscible liquids lead to perturbations in the flow of a liquid jet (Lukas *et al.*, 2010; Riyabi *et al.*, 2012). The interfacial pressure difference is higher in the parts where the jet radius is smaller, compared to the jet parts with bigger radius.

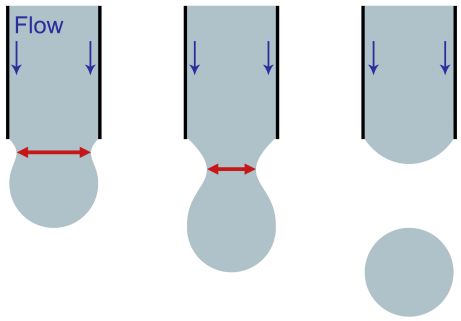

Figure 2.2: Creation and elongation of a "neck" in the jet stream as a droplet is formed. The neck width is indicated with a red arrow.

This results in the increase of the perturbations and the creation of a spherical bulb that is connected to the body of the jet stream via a "neck" (Figure 2.2). The created neck becomes smaller as the fluid flows from the body of the jet and stronger interfacial forces lead to its thinning (Wang *et al.*, 2005). Dispersed droplets are created when the spherical bulb detaches from the jet stream. During this so-called pinch-off process where a droplet is created, secondary, or satellite, droplets might also form (Shabahang *et al.*, 2011). The break-off process however is not yet fully understood due to its complexity as it depends on a combination of many parameters.

The size and the frequency of the formed droplets both depend on the relation between the interfacial and the viscous forces. The droplet size is inversely proportional to the capillary number,

$$R_{drop} = \frac{h}{Ca} = \frac{\gamma h}{\mu v} \tag{2.9}$$

where h is the channel width. The above expression implies that the determination of the droplet size can be complex, as it depends on a combination of several parameters.

Depending on factors such as the surface tension, the viscosity and the external pressure, droplet formation can be distinguished and described by different regimes. The three most commonly encountered regimes are the so called dripping regime, jetting regime and squeezing regime (Seemann *et al.*, 2012), see Figure 2.3. At the dripping regime, monodisperse droplets are formed near the intersection of the two phases, for high Ca numbers (Tarchichi *et al.*, 2013). At the jetting regime droplets are formed at the tip of a jet that is extended "downstream" of the intersection of the two phases (Gor-

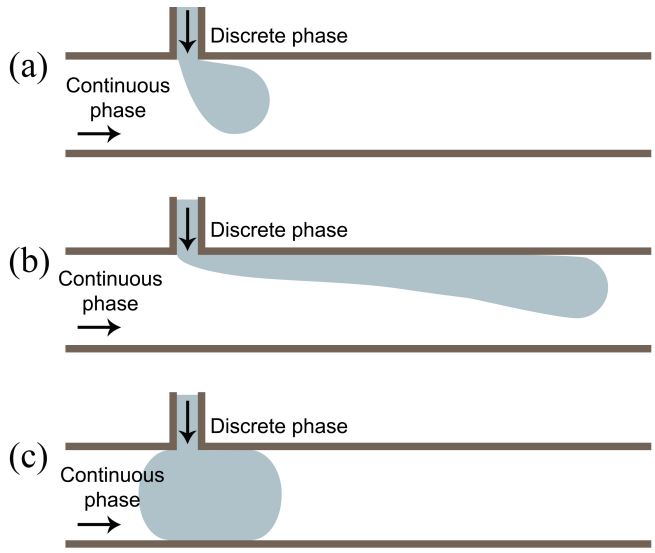

Figure 2.3: Droplet break-off regimes. The dripping regime (a), the jetting regime (b) and the squeezing regime (c).

don and Shelley, 2007). Finally at the squeezing regime the break-off occurs at the interface of the two phases, at low Ca numbers (Tarchichi *et al.*, 2013).

Two basic parameters that influence the formation of droplets as well as the size of the generated droplets are the interfacial tension between the two phases and the viscosity. For this reason, the addition of solvents or other molecules in either the continuous or the discrete phase is a common way to alter the attained surface tension and viscosity and thus to facilitate the droplet formation. For instance, for the case where the two immiscible liquids are water and oil, addition of water-immiscible organic solvents in the oil continuous phase can increase its viscosity thus ease droplet generation (Teh *et al.*, 2008). In addition the value of the interfacial tension specifically for water/oil emulsions can be reduced by the addition in the continuous phase of *i.e.* surfactants; amphiphilic molecules consisting of a hydrophilic and a hydrophobic part. The addition of surfactants into the continuous phase can prevent droplets from coalescing but also alter the wettability of the channel surface (Teh *et al.*, 2008).

References

Beech, J. (2011), Microfluidics - Separation and Analysis of Biological Particles, PhD Thesis, Lund: Lund University.

Bruus, H. (2008), *Theoretical Microfluidics*, Oxford University Press, pp. 3, 23–27, ISBN: 978-0-19-923508-7.

Gordon, C. F. and Shelley, A. L. (2007), Microfluidic methods for generating continuous droplet streams, *J. Phys. D: Appl. Phys.* 40 (19), R319–R336, DOI: 10.1088/0022-3727/40/19/R01.

Holtzman, R., Szulczewski, M. L., and Juanes, R. (2012), Capillary Fracturing in Granular Media, *Phys. Rev. Lett.* 108 (26), 264504(1)–264504(4), DOI: 10.1103/PhysRevLett.108.264504.

Lukas, D., Pan, N., Sarkar, A., Weng, M., Chaloupek, J., Kostakova, E., Ocheretna, L., Mikes, P., Pociute, M., and Amler, E. (2010), Auto-model based computer simulation of Plateau-Rayleigh instability of mixtures of immiscible liquids, *Physica A : Statistical Mechanics and its Applications* 389 (11), pp. 2164–2176, DOI: 10.1016/j.physa.2010.01.046.

Riyabi, A. A., Boutat, M., and Hilout, S. (2012), On the Rayleigh-Plateau instability, *Appl. Math. J. Chinese Univ.* 27 (2), pp. 127–138, DOI: 10.1007/s11766-012-2968-7.

Seemann, R., Brinkmann, M., Pfohl, T., and Herminghaus, S. (2012), Droplet based microfluidics, *Rep. Prog. Phys.* 75 (1), p. 016601, DOI: 10.1088/0034-4885/75/1/016601.

Shabahang, S., Kaufman, J. J., Deng, D. S., and Abouraddy, A. F. (2011), Observation of the Plateau-Rayleigh capillary instability in multi-material optical fibers, *Applied Physics Letters* 99 (16), 161909(1)–161909(3), DOI: 10.1063/1.3653247.

Streets, A. M. and Huang, Y. (2014), Microfluidics for biological measurements with single-molecule resolution, *Current Opinion in Biotechnology* 25, pp. 69–77, DOI: 10.1016/j.copbio.2013.08.013.

Tarchichi, N., Chollet, F., and Manceau, J.-F. (2013), New regime of droplet generation in a T-shape microfluidic junction, *Microfluidics and Nanofluidics* 14 (1–2), pp. 45–51, DOI: 10.1007/s10404-012-1021-8.

Teh, S.-Y., Lin, R., Hungb, L.-H., and Lee, A. P. (2008), Droplet microfluidics, *Lab Chip* 8 (2), pp. 198–220, DOI: 10.1039/B715524G.

Wang, J., Joseph, D., and Funada, T. (2005), Purely irrotational theories of the effects of viscosity and viscoelasticity on capillary instability of a liquid cylinder, *J. Non-Newtonian Fluid Mech.* 129 (2), pp. 106–116, DOI: 10.1016/j.jnnfm.2005.04.003.

3 Deterministic Lateral Displacement

3.1 Overview

The Deterministic Lateral Displacement (DLD) is a method first introduced by Huang *et al.* (2004), that is primarily used for particle separation. A microfluidic device which consists of tilted arrays of micrometer sized posts is used. Particles suspended in a fluid that is running in the device interact with the fixed posts and follow the streamlines or the geometry of the device depending on their characteristics. Such characteristics include their size, shape and softness. Modification of the device geometry, such as the distance between the posts or the post tilt can create additional streamlines which in turn affect the particle separation. Particles in DLD devices are separated spatially and the separation is based on a deterministic process, a characteristic that enables precise and high throughput particle sorting.

To date there exist several microfluidic techniques that are used for particle sorting based on size and deformability. In the microfluidic funnel ratchets for instance (McFaul *et al.*, 2012) small and soft particles, unlike large and rigid ones, get squeezed and flow through the funnels resulting in spatial separation. However clogging of the device is an important disadvantage of this method.

The DLD is on the other hand an emerging, less complex method that is based on the mechanical sorting of particles. It can find applications in biomedicine in several ways, such as in diagnostics, e.g. for separation of parasites from human blood (Holm *et al.*, 2011). It can be also used to provide us with information for the different properties of the cells contained in blood, like their size, deformability, or morphology (Beech *et al.*, 2012; Inglis *et al.*, 2008).

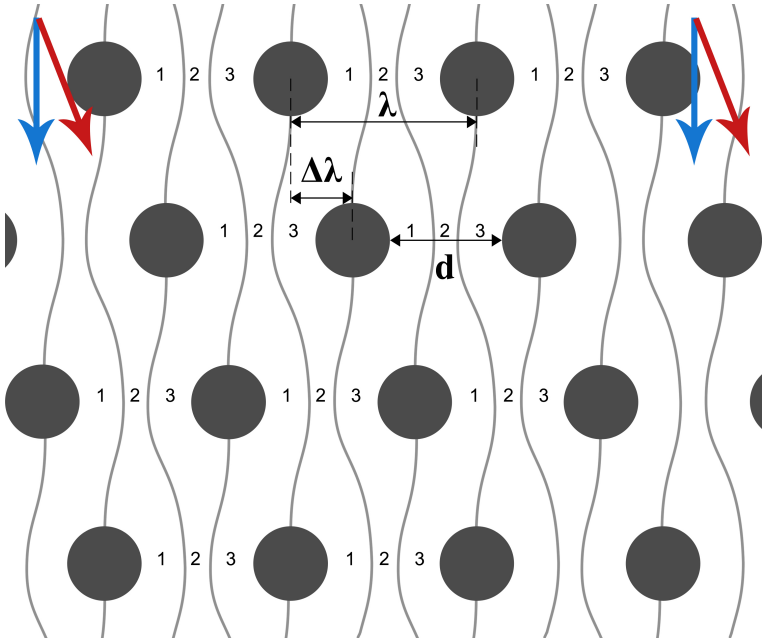

Figure 3.1: The relative shift of a row of posts, $\Delta\lambda$, the center-to-center post distance, λ and the post gap d of a DLD device. The numbers indicate the N indices of the different streamlines. The blue arrows indicate the direction of the flow, whereas the red arrows indicate the direction of the array.

3.2 Particle separation

The DLD device consists of an array of fixed cylindrical micrometer-sized posts. These posts are structured in rows and each row is shifted relatively to the preceding one by an amount of $\Delta\lambda$. The periodicity of the array is described by the number N and depends on the relative shift $\Delta\lambda$ as well as the center-to-center distance of the posts λ:

$$N = \frac{\lambda}{\Delta\lambda} \tag{3.1}$$

The gap between the posts, d, is given by the difference between the center-to-center post distance and the post diameter, as shown in Figure 3.1. A fluid that enters the device will encounter the posts and will be divided into streamlines of different velocities. The number of streamlines depends on the periodicity of the array. In Figure 3.1 for instance three streamlines are created and flow between two posts in the same row. The lines that separate the different streams are known as stall lines. They begin at posts in one period and end at posts in the next one. Consider a post gap that contains N different streamlines. The Nth streamline that crosses two posts will become

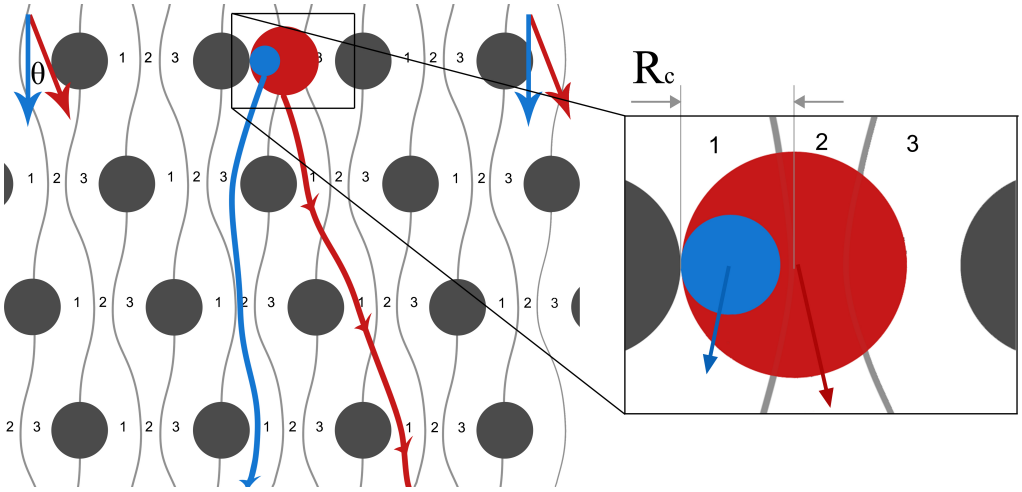

Figure 3.2: Size-based separation in a DLD device: A particle (blue) with radius smaller than the critical radius of the device follows the direction of the flow in a "zig-zag" motion, whereas a particle (red) with a radius bigger than the critical one is displaced by the posts and follows the direction of the array.

streamline with index $N-1$ when it will flow to the next row. One period is complete when the streamline goes back to the Nth position. In Figure 3.1, $N = 3$ and one period is complete when the first streamline, after having crossed several rows of posts, becomes again streamline with index 1.

Particles suspended in the fluid will flow in the streamlines with the same speed, as mentioned in section 2.4. However, the steric interaction of the particles with the fixed posts acts as an external force that can affect their flow. If a particle is small and its center of mass is found inside a streamline of a specific width, it will then remain in the same streamline and will continue flowing in the same direction as the fluid. On the contrary a bigger particle with a radius that exceeds the streamline width will be displaced into the adjacent streamline. The path that a particle will follow in the device is thus dependent on its size as well as on the streamline width. The streamline width depends on the number of streamlines created in the gap which in turn depends on the array periodicity. The width of the first streamline determines the so called critical radius of the device, R_c (Beech *et al.*, 2012). Therefore, particles with a radius smaller than the critical radius will follow the direction of the flow in a "zig-zag" motion, whereas particles with a radius larger than the critical radius will be displaced by the posts by an angle θ relative to the direction of flow, see Figure 3.2. This way spatial separation based on size can be achieved. The angle θ is dependent on the

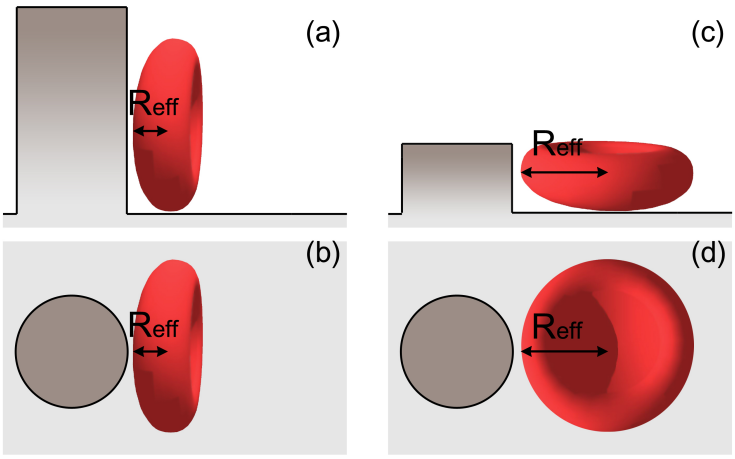

Figure 3.3: Basic principle for shape based sorting. In a deep device a biconcave disk-shaped red blood cell can rotate freely and is separated based on its smaller dimension. The device here is seen in profile (a) and from top (b). On the contrary, in a shallow device a red blood cell is separated based on its bigger dimensions. Illustrated as seen in profile (c) and from top (d).

array periodicity and is given by:

$$\theta = arctan(1/N) \tag{3.2}$$

The critical radius of the device is given by the expression:

$$R_c = \alpha \frac{d}{N} \tag{3.3}$$

where α is a parameter that describes the influence of the parabolic profile between the posts in pressure driven flow. Streams close to the posts are wider than these in between. This is due to the fact that fluid close to the posts flows slower, but the flux is always constant. Hence in parabolic flow α is larger than 1 whereas in the case of plug-like flow α equals 1.

The critical size of a device can also be referred to as the critical diameter, D_c, which is double the size of the critical radius. An experimental approximation is often used to determine the critical radius and is given by the expression (Davis, 2008):

$$R_c = \frac{1.4 d N^{-0.48}}{2} \tag{3.4}$$

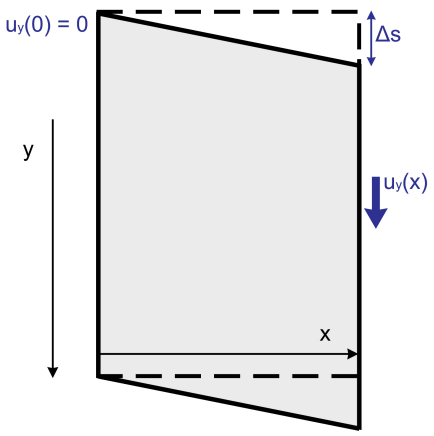

Figure 3.4: Deformation of a fluid due to viscous shear stress.

Particles that are to be separated, especially particles in biological samples, are not always rigid or spherical. This affects their mechanical properties in the device and that in turn determines the path they will follow. For instance, a biconcave disk-shaped red blood cell (RBC) might rotate in the device and exhibit different sizes depending on its orientation, as shown in Figure 3.3. For this reason, an additional factor that can affect the particle separation except for the periodicity and the post gap is the depth of the device. Similarly, deformable particles that interact with the posts might exhibit different mechanical properties compared to these of more rigid particles. This effective size of the particles, R_{eff}, is therefore the one that determines the trajectory that they will follow in the device, depending on its relation with the critical radius.

3.2.1 Deformability-based separation

An external force that is applied on a solid object will induce a deformation, which will in turn lead to the generation of a mechanical stress. For solids the generated stress can either be normal or shear. Normal stress is generated when a force is applied perpendicularly to the surface of the object,

$$\sigma = Y\epsilon \tag{3.5}$$

where Y is the Young's modulus and ϵ is the strain, whereas shear stress is induced by a force parallel to the object's surface,

$$\tau = G\gamma \tag{3.6}$$

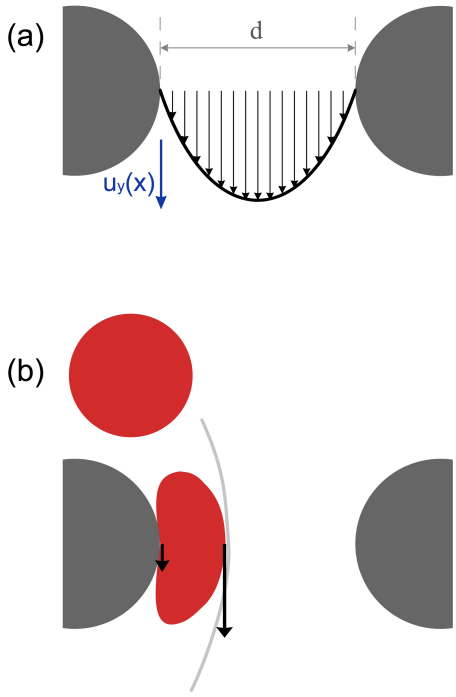

Figure 3.5: Parabolic flow profile between two posts. The flow velocity in the y-direction is a function of the distance from the posts (a). Deformation of a particle caused by a shear stress (b).

where $G = \frac{Y}{2(\epsilon+1)}$ is the shear modulus and γ is the shear strain. Similarly to a solid object, a Newtonian fluid with a constant viscosity that is flowing in a channel will experience a viscous shear stress along the boundaries of the channel. Due to the no-slip condition, the flow will be parabolic, meaning that the speed of the flow at the boundary is zero while the flow speed at the center of the channel is maximized. The shear strain induced by the difference in the flow velocity profile is given by the expression:

$$\gamma(t) = \frac{\Delta s}{x} = \frac{u_y(x)t}{x} \tag{3.7}$$

where Δs is the deformation and $u_y(x)$ is the fluid velocity at the position x (Figure 3.4). A particle travelling in the fluid will also experience a shear stress at the boundaries. These boundaries in the case of the DLD device correspond to the posts of the array (Figure 3.5a). Therefore, a soft and deformable particle that passes between two posts will be deformed and its deformation will be proportional to the applied flow pressure. The shear

stress, τ, in the case of a Newtonian fluid is given by the expression (Darby, 2001):

$$\tau = \mu\dot{\gamma} \tag{3.8}$$

where $\dot{\gamma}$ is the shear strain rate and μ is the viscosity of the fluid. The shear strain rate is given by the derivative of the flow velocity with respect to the displacement in the perpendicular direction, see Figure 3.5a:

$$\dot{\gamma} = \frac{d\gamma}{dt} = \frac{\partial u_y}{\partial x} \tag{3.9}$$

The shear strain rate $\dot{\gamma}$ however should not be confused with the interfacial tension γ. The fluid velocity for a parabolic flow profile in a tube of radius α is given by the expression:

$$u(r) = u_{max}\left(1 - \frac{r^2}{\alpha^2}\right) \tag{3.10}$$

In the case of a DLD device, the maximum velocity of a stream flowing between two posts is reached in their mid-gap and since the velocity depends only on the position in the x-direction, equation 3.10 becomes:

$$u_y = u_{max}\left(1 - \frac{4x^2}{d^2}\right) \tag{3.11}$$

where x is the position in the x-direction and d is the gap between two posts of the device. By substituting equation 3.11 in equation 3.8, we obtain the shear stress at the wall of the post:

$$\tau = 4\mu\frac{u_{max}}{d} \tag{3.12}$$

Since the velocity gradient depends on the position in the x-direction, the part of a particle that is close to a post will move slower, compared to the part that is found at a bigger distance from the post (Figure 3.5b).

As previously mentioned, when dealing with biological samples particles are often soft and deformable. When inside the DLD device such particles interact with the fixed posts, and experience a shear stress. This shear stress deforms the particles and this deformation in turn results in a decrease of their effective size. Hence, a soft particle of a certain shape and size appears

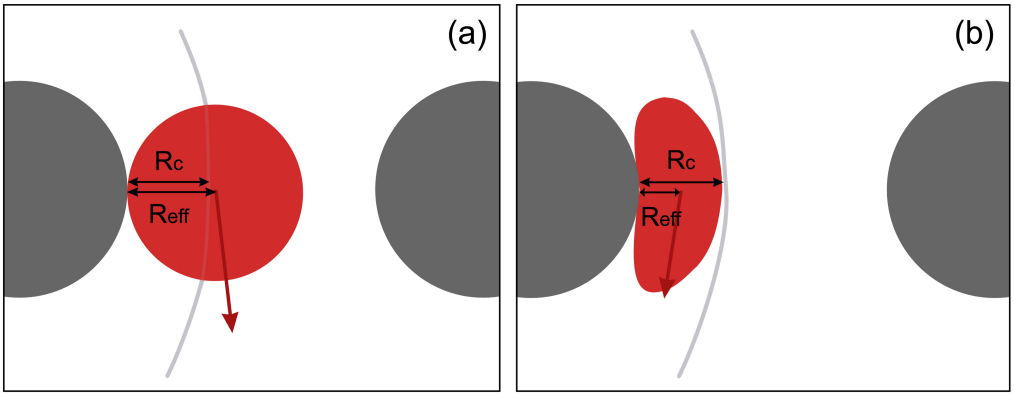

Figure 3.6: Deformability-based separation. A rigid particle has a larger effective radius, R_{eff}, than the critical radius of the device, R_c and is displaced by the posts (a). A deformable particle has a smaller effective radius than the critical one and follows the direction of the flow (b).

smaller than a rigid particle with the same shape and dimensions. The two particles therefore follow a different path in the device (Figures 3.6, 3.7). In Figure 3.8 a finite element simulation of water flow in 2-D, made with COMSOL Multiphysics 4.4, is presented. For the simulation laminar flow and no-slip boundary conditions are used. The dimensions of the array designed for the simulations are presented in Table 3.1. As expected, the simulations indicate that at high applied flow pressures the shear rate, that a particle in the fluid will experience due to interaction with the posts, is stronger than that at lower pressures.

The ability of DLD devices to spatially separate soft particles from more rigid ones is advantageous and has opened up many applications in the field of biomedicine. One example is the study performed by Beech *et al.* (2012) where DLD devices were used for separation of soft red blood cells (RBCs) from rigid ones for diagnostic purposes.

At this point however it is necessary to mention that there are several factors that may reduce the separation resolution and throughput. For instance, running the particles at low flow rates should be avoided in order to minimize diffusion. Particles that flow in low speeds have more time to diffuse, hence diffusion predominates over the deterministic separation. On the other hand, high flow rates might lead to an undesirable increase of the deformation of soft particles which might also lower the resolution. For this reason in pressure-driven flows, flow rates have to be selected accordingly so that

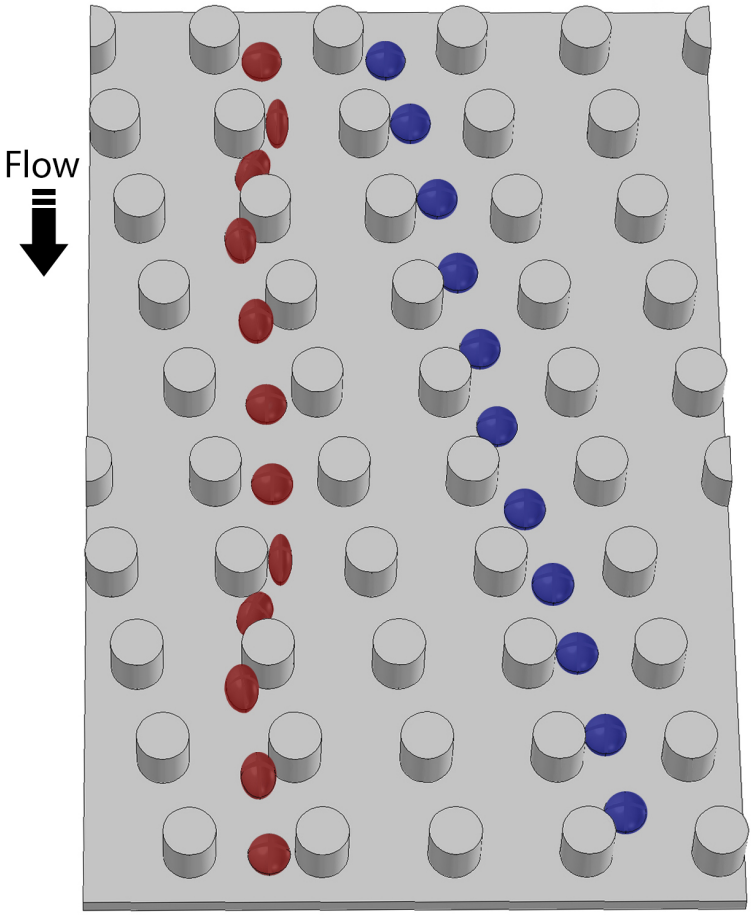

Figure 3.7: Illustration of a soft and a rigid spherical particle in a DLD device; the soft particle (red) is deformed and flows in a "zig-zag" motion, whereas the rigid particle (blue) is displaced by the posts and follows a different trajectory in the device.

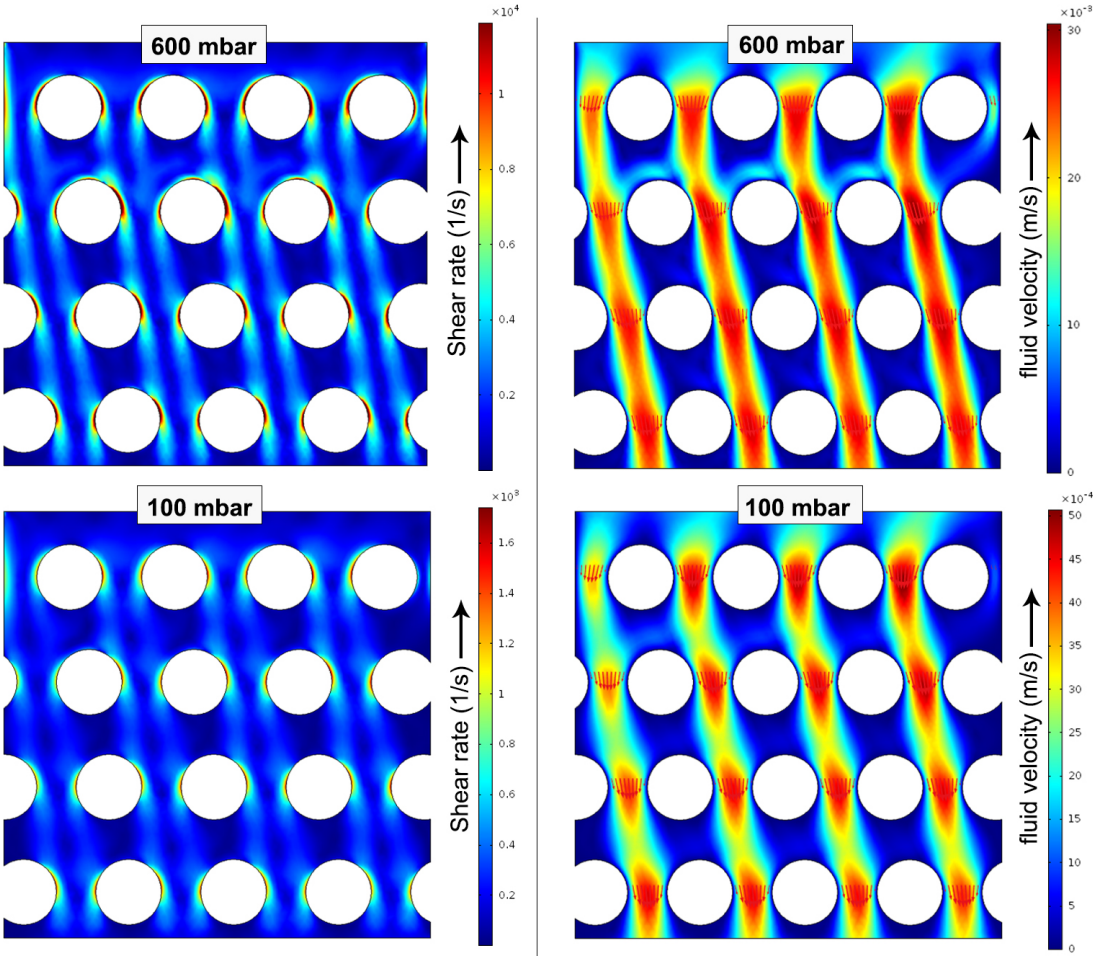

Figure 3.8: A 2-D COMSOL simulation of the shear strain rate and the fluid velocity in a DLD device at applied pressures of 100 mbar and 600 mbar.

Table 3.1: Design parameters for the 2-D COMSOL simulations.

λ	32 μm
d	12 μm
Post radius	10 μm
$\Delta\lambda$	6 μm

the maximum throughput can be achieved.

3.2.2 Simple physical model

A spherical water droplet suspended in oil phase will experience a surface tension, γ, that originates from the water/oil interface. In order for the droplet to be deformed in the DLD device, the applied shear forces must be stronger than the interfacial tension. In this section a theoretical model is presented for the estimation of the shear forces in the DLD required to deform a water droplet in oil. Interfacial tension tends to minimize the water area that is exposed to the oil by retaining the spherical shape of the droplet. It has been shown that a liquid droplet onto which is applied a force, responds as a Hookean spring with a spring constant that is linearly proportional to the surface tension (Attard and Miklavcic, 2001).

We assume a sphere of radius r onto which a point force is applied. By considering a constant volume, the sphere is deformed into an oblate ellipsoid. The energy E_{tot} of the ellipsoid is given by:

$$E_{tot} = S\gamma \tag{3.13}$$

where S is the surface area of the ellipsoid and γ is the interfacial tension. By assuming a constant volume we can express the surface of the ellipsoid as a function of the shortest axis:

$$E(r - \Delta y) = S(r - \Delta y) \cdot \gamma \tag{3.14}$$

where Δy is the deformation in the direction of the force (Figure 3.9). By taking the second-order Taylor series expansion of the energy around $\Delta y = 0$ we can express the energy as $E = constant \cdot (\Delta y)^2$. By subsequently taking the second derivative of the energy with respect to Δy we find the expression for the spring constant, $k = k(\gamma, r)$. For a water droplet in FC-40 oil with surfactants, $\gamma = 52.07$ mN/m and for an initial radius of approximately $r = 5$ μm, we obtain $k = 526$ mN/m. This means that $k \simeq 10\gamma$. However, according to Filip *et al.* (2005), $k \simeq \gamma$. This difference in the estimated k could

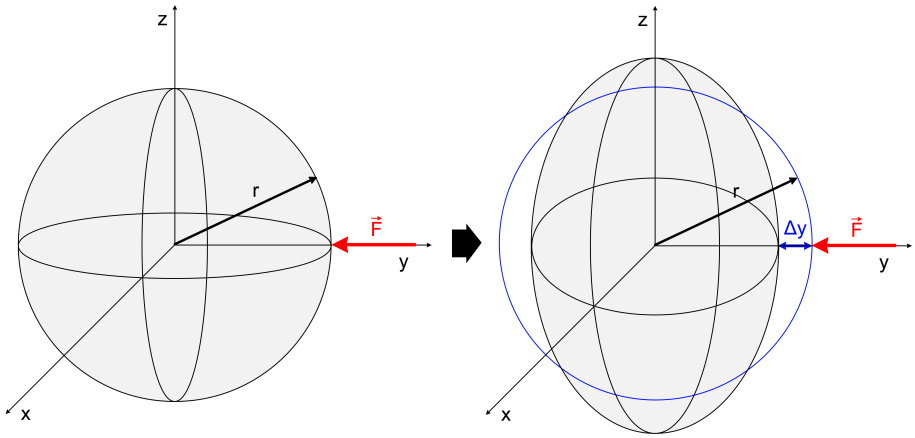

Figure 3.9: A sphere onto which is applied a point force will be deformed into an oblate ellipsoid, assuming a constant volume.

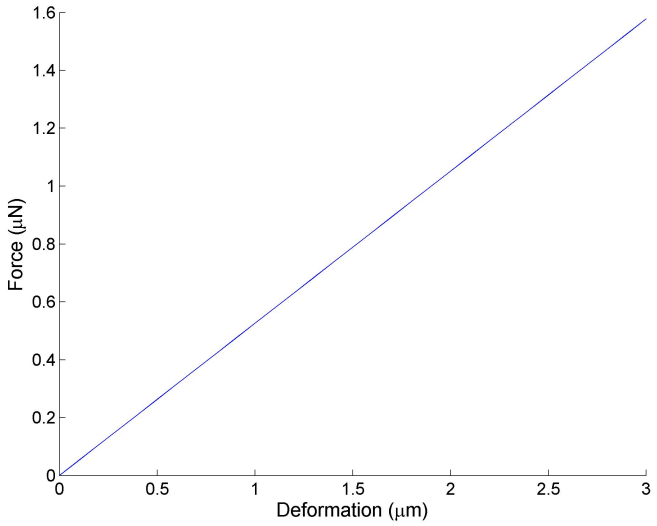

Figure 3.10: Theoretically derived Hooke's law for a sphere that is deformed into an ellipsoid by a point force.

arise from the fact that the approximate formula for the surface area of the ellipsoid was used[1]. Thus, from Hooke's law we obtain the relation between the applied force and the theoretically resulting deformation, see Figure 3.10.

The shear force applied on the droplets due to the interaction with the posts

[1] $S \simeq 4\pi(\frac{(ab)^{1.6}+(bc)^{1.6}+(ac)^{1.6}}{3})^{1/1.6}$

in the DLD device is given by:

$$F = \mu\dot{\gamma}A \tag{3.15}$$

where A is the droplet hemisphere surface.
The viscosity of a 1% agarose gel can be calculated by the total stress for a viscoelastic material:

$$\sigma_{tot} = \sigma_{elastic} + \sigma_{viscous} \Rightarrow F = kx + c\dot{x} \tag{3.16}$$

where F is the applied force, k is the spring constant, c is the damping coefficient and x is the deformation. For a gravitational force $F = mg$ applied on bulk agarose surrounded by FC-40 oil, the damping coefficient is given by $c = \frac{\mu A}{L}$ with μ the viscosity, A the area onto which the force is applied and L the initial height of the agarose. The solution for the differential equation 3.16, is given by:

$$x(t) = a_1 \cdot e^{-\frac{t}{\tau}} + \frac{mg}{k} \tag{3.17}$$

where $\tau = c/k$ is the relaxation time. By assuming that at $t = 0$ there is no deformation and that at $t \to \infty$ the agarose gel has reached its maximum deformation of ΔL, we obtain:

$$k = \frac{mg}{x(t \to \infty)} = \frac{mg}{\Delta L} \tag{3.18}$$

The viscosity is then given by the relaxation time. The physical model will be further discussed and compared to the deformation results in chapter 8.

References

Attard, P. and Miklavcic, S. J. (2001), Effective Spring Constant of Bubbles and Droplets, *Langmuir* 17 (26), pp. 8217–8223, DOI: 10.1021/la010969g.

Beech, J. P., Holm, S. H., Adolfsson, K., and Tegenfeldt, J. O. (2012), Sorting cells by size, shape and deformability, *Lab Chip* 12 (6), pp. 1048–1051, DOI: 10.1039/C2LC21083E.

Darby, R. (2001), *Chemical Engineering Fluid Mechanics*, 2nd ed., Marcel Dekker, Inc., p. 57, ISBN: 978-0824704445.

Davis, J. A. (2008), Microfluidic Separation of Blood Components through Deterministic Lateral Displacement, PhD Thesis, Princeton: Princeton University.

Filip, D., Uricanu, V. I., Duits, M. H. G., Agterof, W. G. M., and Mellema, J. (2005), Influence of Bulk Elasticity and Interfacial Tension on the Deformation of Gelled Water-in-Oil Emulsion Droplets: An AFM Study, *Langmuir* 21 (1), pp. 115–126, DOI: 10.1021/la048276y.

Holm, S. H., Beech, J. P., Barrett, M. P., and Tegenfeldt, J. O. (2011), Separation of parasites from human blood using deterministic lateral displacement, *Lab Chip* 11 (7), pp. 1326–1332, DOI: 10.1039/c0lc00560f.

Huang, L. R., Cox, E. C., Austin, R. H., and Sturm, J. C. (2004), Continuous Particle Separation Through Deterministic Lateral Displacement, *Science* 304 (5673), pp. 987–990, DOI: 10.1126/science.1094567.

Inglis, D. W., Davis, J. A., Zieziulewicz, T. J., Lawrence, D. A., Austin, R. H., and Sturm, J. C. (2008), Determining blood cell size using microfluidic hydrodynamics, *J. Immunol. Methods* 329 (1–2), pp. 151–156, DOI: 10.1016/j.jim.2007.10.004.

McFaul, S. M., Lina, B. K., and Ma, H. (2012), Cell separation based on size and deformability using microfluidic funnel ratchets, *Lab Chip* 12 (13), 2369—2376, DOI: 10.1039/c2lc21045b.

4 Droplet-based microfluidics for particle synthesis

4.1 Applications

As mentioned earlier, droplet-based microfluidic systems are a sub-category of microfluidic technology and involve the formation of droplets using the co- or cross- flow of two immiscible liquids under laminar flow conditions. The volumes of the created droplets are most commonly in the range of picoliters to nanoliters and their diameters can vary from hundrends of nanometers to tens of micrometers. In addition, the frequency of droplet generation can be as high as some tens of kHz. These systems are tools with which the droplet size, and generation frequency can be controlled. Individual droplets can also be transported, mixed, split and sorted for high throughput synthesis and analysis (Teh *et al.*, 2008). Control over their characteristics can be attained by regulating the external pressures applied but also by using droplet-based devices with geometries appropriate for the individual applications. At the microscale, diffusion distances as well as the required mass transfer times are decreased. This characteristic enables the use of droplets as microreactors where several parallel reactions can be controlled and performed at a short time. In the studies demonstrated by Kim *et al.* (2012) and Sakakihara *et al.* (2010), droplet-based microfluidics were used in enzymatic assays for the investigation of the activity and the detection of single enzymes.

Encapsulation of individual cells in droplet particles is also a very powerful tool that finds many applications in the fields of diagnostics and pharmaceuticals. In a study performed by Streets and Huang (2013), droplet systems were used for the investigation of quorum sensing in bacterial cells (initiation of signal exchange at high cellular concentrations). The concentration of cells encapsulated in a volume of a few nano- or picoliters is relatively higher than that of cells in a bulk solution. The diffusion distances for the

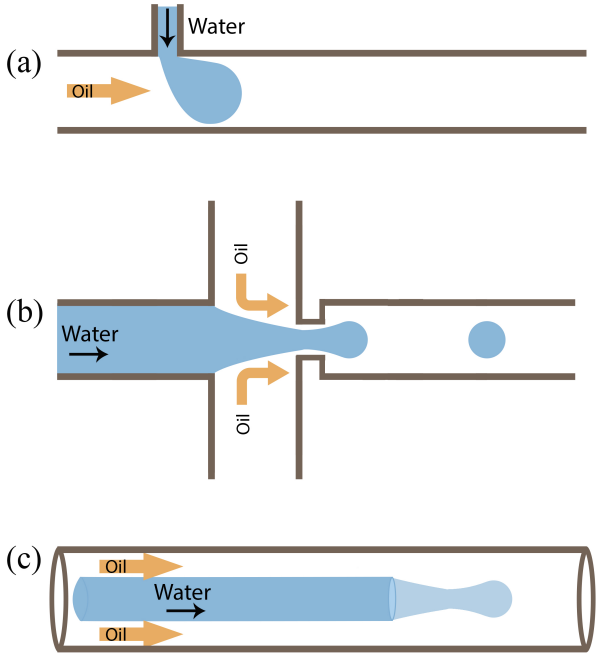

Figure 4.1: Illustration of droplet generation at the dripping regime in the different device designs. A T-junction (a), a flow-focusing (b) and a co-flow (c) device.

secreted substances inside the droplets are decreased. This in turn results in the activation of quorum sensing, which, with the aid of droplet-based technology, can be investigated at the single-cell level.

4.2 Device design and characteristics

The generation of droplets and their final size depend on the device geometry as well as surface chemistry. For the production of droplets, the two phases are driven into microchannels via independent applied pressures (Gordon and Shelley, 2007).

The device geometries most commonly used for droplet generation are characterized by the relative flow of the immiscible phases in the device. Such geometries include the T-junction, the flow-focusing and the co- flow (Gordon and Shelley, 2007). In the T-junction geometry, the break-up process is based on the cross- flow of the two immiscible streams. The microchannel that contains the disperse phase perpendicularly intersects the microchannel containing the continuous phase (Teh *et al.*, 2008), see Figure 4.1a. In the flow-focusing geometry, the break-up process relies on the focusing of the

dispersed stream. The microchannel containing the dispersed phase intersects perpendicularly two microchannels that contain the continuous phase, as shown in Figure 4.1b. This way the dispersed phase experiences symmetric shear forces by the second phase. The forces in turn focus the disperse stream and force it through a narrow area in the device, the nozzle. Droplets are then broken-off downstream from the nozzle. Finally, in the co- flow geometry the break-up process is based on the co- flow of the two immiscible liquids. A stream of the dispersed phase is surrounded by a co- flowing stream of the continuous phase (Figure 4.1c). In the co- flow design no nozzle is used and the discrete phase breaks into droplets directly into a wide channel. In all cases, the size of the created drops strongly depends on the type of the geometry but also on the dimensions of the channels and the nozzles.

In the current project a flow-focusing device of 13 μm depth and 2.4 cm length is used for the synthesis of droplets (Figures 4.2a-d). For the injection of the two immiscible phases into the device and also for the collection of the generated droplets, inlet and outlet reservoirs are connected to the microchannels of the device. In Figure 4.3 an SEM image of the junction of the flow-focusing device is shown.

Another important device characteristic that has to be considered for the formation of droplets is its surface chemistry. The generated droplets are surrounded by the continuous phase which wets the channel walls of the device. For this reason, in order to prevent the dispersed phase from adhering to the channel walls, the device must be surface-treated according to the nature of the continuous phase. For instance, for water/oil emulsions where water droplets are formed in a continuous oil phase, hydrophobic channels are required. On the contrary for oil/water emulsions the channels have to be hydrophilic. One of the most commonly used treatments for making a device hydrophobic is the silanization using alkane silanes. More on the surface treatments are discussed in 7.1 and in the Appendix.

4.3 Encapsulation of particles

As previously mentioned, the encapsulation and manipulation of particles in droplets is one of the biggest advantages of droplet-based microfluidic systems. It is a very powerful tool that opens up many applications for droplet-based systems, for instance for the investigation of different reactions and other processes at the single-cell level. In most single-cell studies the encapsulation of a single cell in each droplet is therefore essential. However,

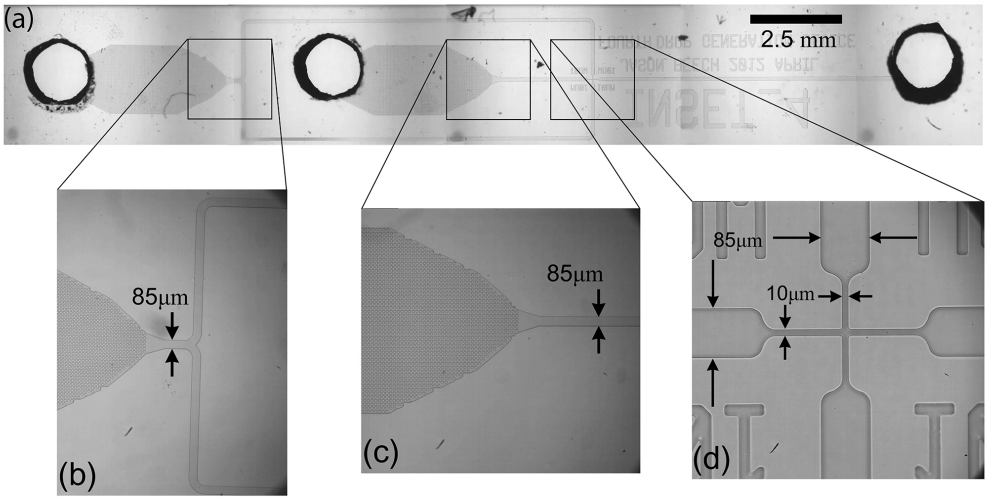

Figure 4.2: (a) The flow focusing device used for the generation of droplets, as seen under the microscope at the bright field mode with a 1x objective. Three holes are punched at the inlets and the outlet of the device, where the reservoirs will be attached. (b) The inlet where the oil is injected, as seen with a 4x objective. (c) The inlet where the aqueous phase is injected, as seen with a 4x objective. (d) The junction of the device, where the microchannels of the oil and the aqueous phases are perpendicularly intersected. Image acquired with a 20x objective.

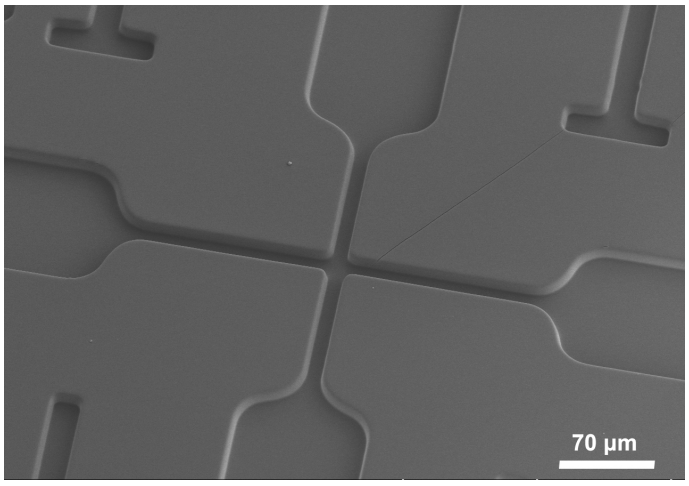

Figure 4.3: An SEM image of the junction of the flow focusing device.

the encapsulation of particles in droplets is random and the distribution of the particles in each droplet follows the Poisson distribution. The probability mass function of the random variable X is given by:

$$f(k, \lambda) = P(X = k) = \frac{\lambda^k e^{-\lambda}}{k!} \tag{4.1}$$

where k is the number of particles per drop for $k = 0, 1, 2, ...$, $\lambda = <k>$ and $P(X = k)$ is the probability for the encapsulation of a certain number of particles per droplet. For single-cell studies, it is essential that only one cell is encapsulated each time. Due to the Poisson distribution however, the probability that more than one cell is contained in one droplet is also high. For this reason, k is chosen to be close to zero and cell samples are diluted several times, which results in a large number of droplets containing no cells.

Another factor to be taken into consideration in single-cell studies is the toxicity level of the discrete phase. In studies where encapsulation of cells or other micro-organisms is required, it is essential that their survival and, in some cases, their proliferation within the droplets are ensured. Towards this direction, Clausell-Tormos *et al.* (2008) performed a viability assay where they tested the viability of human cells as well as of the multicellular organism *Caenorhabditis elegans* in aqueous droplets formed in droplet-based microfluidic systems.

References

Clausell-Tormos, J., Lieber, D., Baret, J.-C., El-Harrak, A., Miller, O. J., Frenz, L., Blouwolff, J., Humphry, K. J., Köster, S., Duan, H., Holtze, C, Weitz, D. A., Griffiths, A. D., and Merten, C. A. (2008), Droplet-based microfluidic platforms for the encapsulation and screening of mammalian cells and multicellular organisms, *Chemistry & biology* 15 (5), pp. 427–437, DOI: 10.1016/j.chembiol.2008.04.004.

Gordon, C. F. and Shelley, A. L. (2007), Microfluidic methods for generating continuous droplet streams, *J. Phys. D: Appl. Phys.* 40 (19), R319–R336, DOI: 10.1088/0022-3727/40/19/R01.

Kim, S. H., Iwai, S., Araki, S., Sakakihara, S., Iino, R., and Noji, H. (2012), Large-scale femtoliter droplet array for digital counting of single biomolecules, *Lab Chip* 12 (23), pp. 4986–4991, DOI: 10.1039/C2LC40632B.

Sakakihara, S., Araki, S., Iino, R., and Noji, H. (2010), A single-molecule enzymatic assay in a directly accessible femtoliter droplet array, *Lab Chip* 10 (24), pp. 3355–3362, DOI: 10.1039/C0LC00062K.

Streets, A. M. and Huang, Y. (2013), Chip in a lab: Microfluidics for next generation life science research, *Biomicrofluidics* 7 (1), pp. 011302.1–011302.23, DOI: 10.1063/1.4789751.

Teh, S.-Y., Lin, R., Hungb, L.-H., and Lee, A. P. (2008), Droplet microfluidics, *Lab Chip* 8 (2), pp. 198–220, DOI: 10.1039/B715524G.

5 Hydrogels

5.1 Characteristics

Gels are jelly-like colloids that are formed when a liquid is dispersed in a solid. They are structures that consist of synthetic or natural polymeric cross-linked networks and "depending on their flow behavior in steady-state they are categorized as weak or strong" (Gulrez *et al.*, 2011), see Figure 5.1. These polymers can be either made of natural materials and polysaccharides, *i.e.* agarose, or of synthetic materials, *i.e.* polyethylene glycol (PEG). Hydrogels constitute a special category of gels and the prefix "hydro" refers to the capability of these types of gels to take up large amounts of water (Gulrez *et al.*, 2011). The backbone of these three-dimensional polymeric networks in addition consists of specific hydrophilic groups that confer the ability exhibited by the hydrogels to absorb water (Okay, 2010). Therefore the polymer plays the role of the hydrogel matrix and the contained water enables the diffusion of other molecules into and out of the gel, a property that renders hydrogels a very useful tool for numerous applications.

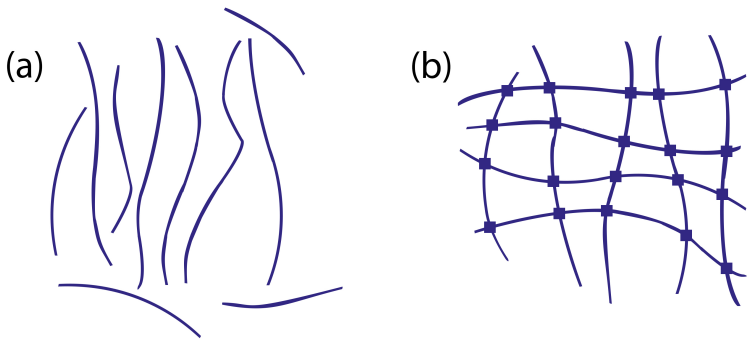

Figure 5.1: Polymer chains (a) and a cross-linked polymeric network (b).

5.1.1 Network formation

When a liquid is dispersed into a solid, the polymeric chains are initially linked together into larger polymeric molecules. Then, in the case of hydrogels, the water absorption leads to a swelling of the network. During that stage, the material is in the so called sol state. Further cross-linking will result in a stronger network formation, the gel. This process is known as gelation or sol-gel transition and the temperature at which the transition occurs is the so called gel point. The sol-gel transition as well as the gel point mainly depend on the chemical characteristics and the concentration of the used polymer. Additionally, the polymer concentration can directly affect the final gel properties, such as its hardness or its elasticity (Okay, 2010). Further cross-linking of the network for transition from sol to gel, usually occurs by either physical or chemical means (Gulrez *et al.*, 2011). Physical methods for gelation include cross-linking by heating/cooling the polymer solution or hydrogen bonding, while chemical methods include the use of chemical cross-linkers. In a big range of applications "control over the mechanical behaviour of hydrogels" is a very useful tool as their gelation point can be chosen accordingly, depending on the needs of each application (Kuckling *et al.*, 2010).

5.1.2 Properties

As previously mentioned, depending on their nature and chemistry, hydrogels may exhibit various properties and characteristics. One of the most important properties of hydrogels is their biocompatibility, that refers to their compatibility to biological organisms (Gulrez *et al.*, 2011). Additionally the high hydrophilicity of hydrogels prevents hydrophobic cells and proteins from adhering to their surface.

Another notable characteristic of the hydrogels is their ability to disintegrate, depending on whether their network is degradable (Gulrez *et al.*, 2011). The degradation of the network often occurs by breakdown of the polymer bonds caused by an enzymatic reaction known as enzymatic hydrolysis. For instance, hydrolysis might occur by enzymes that are specific for a certain polymer-substrate and that cleave the polymeric chains. The breakdown response is therefore dependent on the enzyme concentration as well as on the concentration of the cleavable substrate (Wilson and Guiseppi-Elie, 2013). Breakdown of the polymer chains during gel hydrolysis leads to the formation of smaller molecules and this in turn results in a weakening of the network strength. This effect can be seen as a reverse sol-gel transition. The loss

of polymeric network strength results in a loss of the gelling power of the hydrogel (Armisén and Galatas, 2009).

An additional feature that makes hydrogels a very useful tool for several applications is the ability of some to display a volume change as a response to external environmental stimuli (Gulrez *et al.*, 2011). Such external factors include for instance the external pH, temperature or ionic concentration and can trigger a swelling or shrinking response of the hydrogel, by perturbing its equilibrium.

5.2 Hydrogels as Biosensors

Biosensors are functional tools that in the past years find applications in several fields, such as in biomedicine and biotechnology. However there is an emerging need for creation of simpler and smaller biosensing systems and tools. For this reason, hydrogels are used as biosensors in several applications, *i.e.* as sensing materials that exhibit mechanical signals when there is a change in their environmental conditions. Furthermore, the ability of some hydrogels to disintegrate when they encounter a specific analyte (*i.e.* enzyme or antigen) also enables their use in several applications such as in drug delivery. Current biomedical applications of degradable gels include "feedbacked systems consisting of glucose-sensitive gels that induce insulin release" (Urban and Weiss, 2010; Wilson and Guiseppi-Elie, 2013).

5.3 Agarose

In the current work an agarose polymer is used as the biosensing material. Agarose belongs to the category of natural polymers; it is a linear polysaccharide polymer of molecular weight 120 kDa (Rochas, 1989). It is generally extracted from seaweed (Smith, 1998) and together with agaropectin they compose agar (DeMaria *et al.*, 2013). Agarose is a biocompatible material that can gelify after taking on large amounts of water. Therefore it finds several applications in the field of biomedicine, such as in electrophoresis, in drug delivery and in tissue engineering.

5.3.1 Structure

Agarose is a solid polymer that consists of alternating β-D-galactopyranosil and 3,6-anhydro-α-L-galactopyranosil groups (DeMaria *et al.*, 2013). These

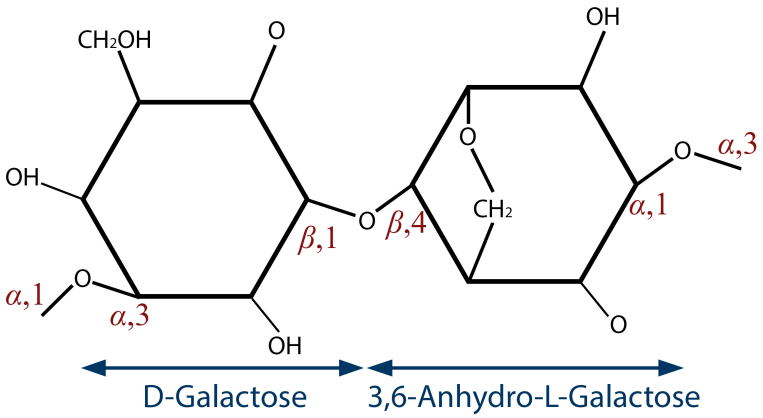

Figure 5.2: The repeated structure unit of the agarose polymer. D-galactose groups are connected through 1,3-α links, whereas 3,6-anhydro-L-galactose groups are connected through 1,4-β links.

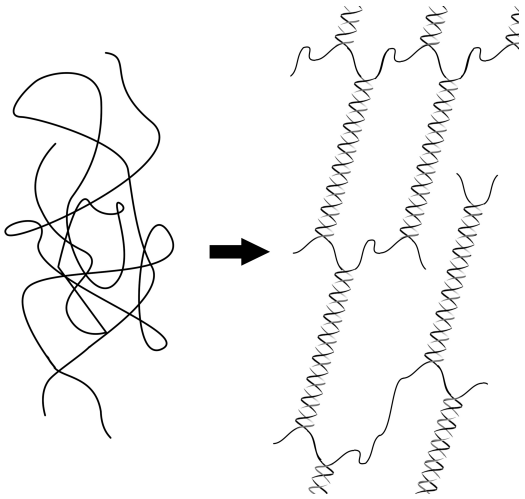

Figure 5.3: Gelation mechanism of agarose. A polymeric network is formed by joined helices when water is added in the agarose and after the mixture is cooled down.

groups make up an entity that repeats throughout the polymer. The components of the β-D-galactopyranosil groups are connected through 1,3-α glycosidic links while the 3,6-anhydro-α-L-galactopyranosil components are connected through 1,4-β linkages (Vera *et al.*, 1998), see Figure 5.2. For the gelation of the agarose the polymeric chains initially couple into double helices that are then joined and form the polymeric network (Stanley, 2006) (Figure 5.3). Absorption of water leads to stabilization of the helices that retain the water and this way the gel is formed.

5.3.2 Properties

Agarose is usually found in the form of a white powder. For preparation of the agarose gel, the agarose polymers are initially mixed with water or other aqueous solvents (Stanley, 2006). The next step is to heat up the solution; this way the polymer forms networks and thereafter reaches the sol state. Transition of the polymer from the sol to the gel state occurs by allowing the mixture to cool down. The polymeric solution has to be heated up at temperatures higher than the gel point in order to compose a sol or in order to melt after having been gelified. This "difference between the melting and gelling point" of agarose gels is the so called "gelation hysteresis effect" (Stanley, 2006). Different agarose types, like high melting point (HMP) or ultra low melting point (ULMP), might exhibit variations in their gelling and melting temperatures. Since the agarose state is inextricably linked with the solution's viscosity at each point, it is presumed that the viscosity will also have a time-temperature dependence. The concentration of the polymer can additionally affect the viscosity of the resulting gel. Depending on the polymeric concentration, there might be some alterations in the macrostructure of the gel, such as changes in the size of the existing pores in the gel matrix (Smith, 1998). The size of these pores usually lies within the range of 100 nm to 700 nm and depends on the agarose concentration (Narayanan *et al.*, 2006). Typical concentrations are found in the range of 0.1-3% w/v of agarose in aqueous solution.

Agarose polymers can produce strong gels, however enzymatic or chemical degradation of the network might result in cleavage of the agarose chains. Degradation of agarose is known to occur enzymatically usually by bacteria collected from marine environments. These types of bacteria are specific for producing particular types of enzymes that can cleave the agarose chains, as it will be further discussed in the following sections.

References

Armisén, R. and Galatas, F. (2009), Agar, *Handbook of hydrocolloids*, ed. by G. O. Phillips and P. A. Williams, Madrid: Woodhead Publishing Series in Food Science, Technology and Nutrition, pp. 21–40, ISBN: 978-1-84569-587-3.

DeMaria, C., Rincon, J., Duarte, A. A., Vozzi, G., and Boland, T. (2013), A new approach to fabricate agarose microstructures, *Polym. Adv. Technol.* 24 (10), pp. 895–902, DOI: 10.1002/pat.3162.

Gulrez, S. K. H., Al-Assaf, S., and Phillips, G. O. (2011), Hydrogels: Methods of Preparation, Characterisation and Applications, *Progress in Molecular and Environmental Bioengineering - From Analysis and Modeling to Technology Applications*, ed. by A. Carpi, Wrexham: InTech, pp. 117–150, ISBN: 978-953-307-268-5.

Kuckling, D., Arndt, K.-F., and Richter, S. (2010), Synthesis of Hydrogels, *Hydrogel Sensors and Actuators*, ed. by G. Gerlach and K.-F. Arndt, Springer Series on Chemical Sensors and Biosensors, Springer Berlin Heidelberg, pp. 15–67, ISBN: 978-3-540-75645-3.

Narayanan, J., Xiong, J.-Y., and Liu, X.-Y. (2006), Determination of agarose gel pore size: Absorbance measurements vis a vis other techniques, *Journal of Physics: Conference Series* 28 (1), pp. 83–86, DOI: 10.1088/1742-6596/28/1/017.

Okay, O. (2010), General Properties of Hydrogels, *Hydrogel Sensors and Actuators*, ed. by G. Gerlach and K.-F. Arndt, Springer Series on Chemical Sensors and Biosensors, Springer Berlin Heidelberg, pp. 1–14, ISBN: 978-3-540-75645-3.

Rochas, C. (1989), Average molecular weight and molecular weight distribution of agarose and agarose-type polysaccharides, *Carbohydrate Polymers* 10 (4), pp. 289–298, DOI: 10.1016/0144-8617(89)90068-4.

Smith, D. R. (1998), Gel Electrophoresis of DNA, *Molecular Biomethods Handbook*, ed. by R. Rapley and J. M. Walker, Humana Press, pp. 17–33, ISBN: 978-1-59259-642-3.

Stanley, N. F. (2006), Agars, *Food Polysaccharides and Their Applications*, ed. by A. M. Stephen, G. O. Phillips, and P. A. Williams, New York: Taylor and Francis Group, pp. 217–238, ISBN: 978-0-8247-5922-3.

Urban, G. A. and Weiss, T. (2010), Hydrogels for Biosensors, *Hydrogel Sensors and Actuators*, ed. by G. Gerlach and K.-F. Arndt, Springer Series on Chemical Sensors and Biosensors, Springer Berlin Heidelberg, pp. 197–220, ISBN: 978-3-540-75645-3.

Vera, J., Alvarez, R., Murano, E., Slebe, J. C., and Leon, O. (1998), Identification of a Marine Agarolytic *Pseudoalteromonas* Isolate and Charac-

terization of Its Extracellular Agarase, *Appl. Environ. Microbiol.* 64 (11), pp. 4378–4383.

Wilson, N. A. and Guiseppi-Elie, A. (2013), Bioresponsive Hydrogels, *Advanced Healthcare Materials* 2 (4), pp. 520–532, DOI: 10.1002/adhm.201200332.

6 Bacteria

6.1 Characteristics

Bacteria are prokaryotic microorganisms whose sizes and shapes may vary significantly among different types. Some of the most commonly encountered bacteria are *i.e.* rod-like, spherical, or spiral-like (Cabeen and Jacobs-Wagner, 2005). The human body usually contains a large number of several bacterial types. The majority of these bacteria are harmless or even essential for the organism, nevertheless, there are several bacterial types that are pathogens and can cause diseases in the organisms they infect.

In Figure 6.1 a typical bacterial cell structure is illustrated. A bacterium usually consists of three different parts; the protoplasm, the cytoplasmic membrane and the cell wall (Silhavy *et al.*, 2010). A major difference between bacteria and eukaryotic cells is that since bacteria are prokaryotic organisms, they lack a nucleus; their genetic material is directly contained in the protoplasm. In order to move, bacteria generally make use of extracellular structures like *i.e.* flagella and pili. Another important characteristic of

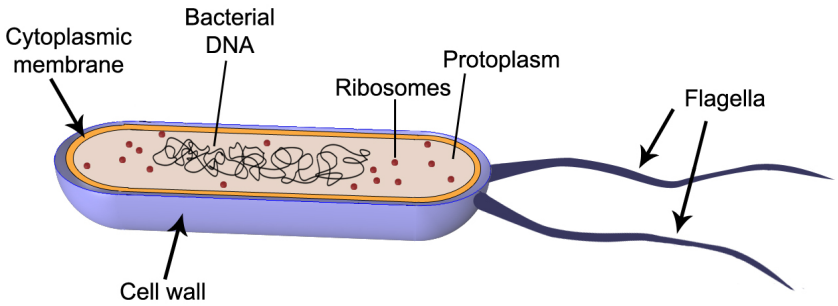

Figure 6.1: Bacterial structure.

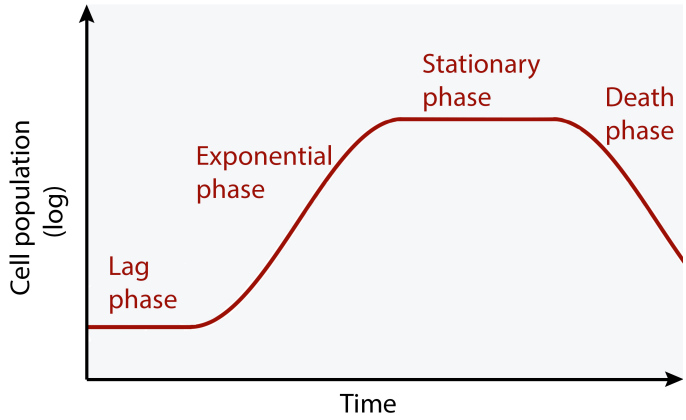

Figure 6.2: Bacterial standard growth curve.

some types of bacteria is their ability to undergo sporulation as a response to extreme environmental conditions, *i.e. Bacillus subtilis*.

6.1.1 Bacterial metabolism and growth

Metabolism of an organism includes all the biochemical reactions that take place inside it. For bacteria, enzymes within the cells are responsible for catalyzing the biochemical reactions, *i.e.* oxidation of substrates, that help them produce energy. Bacterial growth, which refers to the division of a cell into two daughter cells, begins when the mother bacterium reaches its average size. Once its maximum size is reached, the bacterium will grow in a process called binary fission (Buchanan, 1928). During growth a single bacterium increases its cellular mass by forming bacterial colonies. The number of cells can be plotted as a function of time and the resulting curve is the so called standard growth curve. Cell division in general follows an exponential behaviour. The bacterial population at time t, N_t, is thus given by the expression (Buchanan, 1928):

$$N_t = N_0 \cdot 2^n \tag{6.1}$$

where N_0 is the initial population and n is the number of generations at time t. The bacterial growth can be separated in four phases (Figure 6.2). During cell cultivation an amount of bacteria that are grown in a primary medium are taken for the inoculation of a new growth medium. During that stage, known as the lag phase, bacteria do not divide as they are trying to adapt to the new conditions (Yates and Smotzer, 2007). The next phase begins when the bacteria start the replication process. At this stage, bacteria have

reached their maximum size and they start dividing exponentially until all nutritional sources are exhausted. This stage is known as the exponential or logarithmic phase and it typically lasts for 24 to 30 hours. Once all nutrients are consumed, bacteria will enter the stationary phase. During this phase, the number of bacteria in the medium remains constant. This results in the appearance of extreme conditions for the cells (Galdieri *et al.*, 2010). As response to these conditions bacteria might undergo sporulation or express and secrete different types of proteins. During the final stage, the death phase, bacteria do not divide. Those of which that do not form endospores begin to die due to the extreme prevailing conditions.

6.2 Bacterial secretion

Secretion by bacteria is one of the most important processes for the cells' function and it can serve different purposes. Initially, as previously mentioned, it is one of the defensive responses that bacteria exhibit at unfavourable environmental conditions. It is also used to facilitate nutrient uptake. Through secretion bacteria can exchange signals amongst themselves for communication in a process known as quorum sensing (Miller and Bassler, 2001). During quorum sensing the secreted substances work as signals that indicate an increase in the concentration of similar or different bacterial cells in a certain area. Bacteria receive those signals and regulate their gene expression so that they can function as a whole. Many cells also use secretion after invading a host organism as a means of resisting its immune response and colonizing it (Leid *et al.*, 2009), *i.e.* by forming biofilms. The expressed substances in general include several types of proteins and enzymes, but also virulence factors like toxins and adhesins in the case of pathogenic bacteria (Cheung *et al.*, 2000).

6.3 *Pseudoalteromonas atlantica*

6.3.1 Characteristics

Pseudoalteromonas (also known as *Pseudomonas*) *atlantica* are aerobic bacteria that belong to the category of rod-shaped, gram-negative and non spore-forming types. They have a size of approximately 0.5 × 0.2-1.5 × 1.8-4 μm^3 (Mikhailov *et al.*, 2006) (Figures 6.3, 6.4). They are bacteria harmless to humans and in order to move, they make use of extracellular flagella. They are most commonly found in marine environments and are known for producing

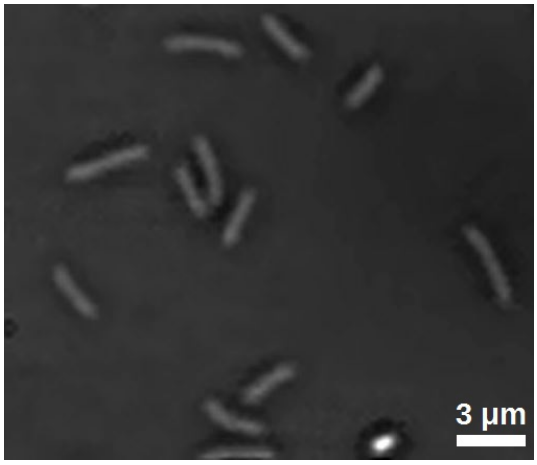

Figure 6.3: *Pseudomonas atlantica* bacteria as seen under the bright field microscope with a 60x objective.

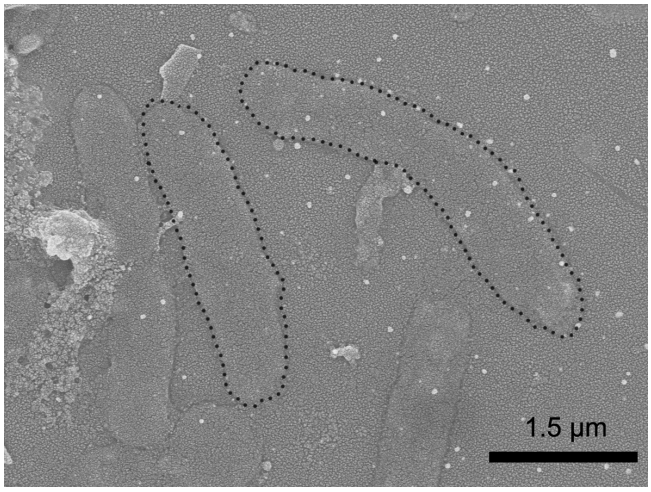

Figure 6.4: SEM image of *Pseudomonas atlantica* bacteria. Two bacteria are highlighted by dotted lines for a better visualization.

and also secreting several types of substances. Such compounds include enzymes like agarase that, as mentioned, can hydrolyze agar and its derivatives. This way the bacteria can take up nutrients such as sugars. *Pseudomonas atlantica* are quorum sensing bacteria that are also known for their ability to form biofilms once they attach to a surface. In order to achieve that, they initially generate energy by utilizing the products from the hydrolysis of their substrates. After forming the biofilms they then produce extracellular polysaccharide (EPS) that in turn provides the colony with additional substrates (Cheung *et al.*, 2000).

6.3.2 Bacterial hydrolysis of agarose

In the current work agarase enzymes secreted by *Pseudomonas atlantica* bacteria are the substances of interest. Agarase enzymes are molecules of size within the range of 20 kDa - 360 kDa (Fu and Kim, 2010) and are known for their ability to hydrolyze agar products. They are commonly secreted by bacteria belonging into the family of *Pseudomonas*, usually when they enter their stationary phase (Malmqvist, 1978). Beta-agarase and alpha-agarase are two types of agarase enzymes, specific for the agarose substrate. Beta-agarase cleaves the 1,4-β links of the 3,6-anhydro-α-L-galactopyranosil groups while α-agarase cleaves the 1,3-α links of the β-D-galactopyranosil groups (Chi *et al.*, 2012). During the breakdown, initially smaller molecules with molecular weight in the range of 10^4 to 10^5 Da are formed and this as mentioned results in a weakening of the gel strength. Further hydrolysis results in the appearance of neoagaro- oligosaccharide and agaro- oligosaccharide molecules as products (Malmqvist, 1978; Chi *et al.*, 2012).

In agarose hydrolysis assays the agarase activity is most commonly detected by using an iodine dye. Iodine is usually sprayed on agarose culture plates where agarose degrading bacteria are grown. Agarase production from the bacteria leads to failure of iodine to stain agarose. Therefore the lack of color increases the contrast and enables the determination of agarase activity.

References

Buchanan, R. E. (1928), Growth Curves of Bacteria, *The Newer Knowledge of Bacteriology and Immunology*, ed. by E. O. Jordan and I. S. Falk, Chicago: University of Chicago Press, pp. 46–57.

Cabeen, M. T. and Jacobs-Wagner, C. (2005), Bacterial cell shape, *Nature Reviews Microbiology* 3 (8), pp. 601–610, DOI: 10.1038/nrmicro1205.

Cheung, H. Y., Sun, S. Q., Sreedhar, B., Ching, W. M., and Tanner, P. A. (2000), Alterations in extracellular substances during the biofilm development of *Pseudomonas aeruginosa* on aluminium plates, *Journal of Applied Microbiology* 89 (1), pp. 100–106, DOI: 10.1046/j.1365-2672.2000.01083.x.

Chi, W. J., Chang, Y. K., and Hong, S. K. (2012), Agar degradation by microorganisms and agar-degrading enzymes, *Appl. Microbiol. Biotechnol.* 94 (4), pp. 917–930, DOI: 10.1007/s00253-012-4023-2.

Fu, X. T. and Kim, S. M. (2010), Agarase: Review of Major Sources, Categories, Purification Method, Enzyme Characteristics and Applications, *Mar. Drugs* 8 (1), pp. 200–218, DOI: 10.3390/md8010200.

Galdieri, L., Mehrotra, S., Yu, S., and Vancura, A. (2010), Transcriptional Regulation in Yeast during Diauxic Shift and Stationary Phase, *OMICS* 14 (6), pp. 629–638, DOI: 10.1089/omi.2010.0069.

Leid, J. G., Kerr, M., Selgado, C., Johnson, C., Moreno, G., Smith, A., Shirtliff, M. E., O'Toole, G. A., and Cope, E. K. (2009), Flagellum-Mediated Biofilm Defense Mechanisms of Pseudomonas aeruginosa against Host-Derived Lactoferrin, *Infect. Immun.* 77 (10), pp. 4559–4566. DOI: 10.1128/IAI.00075-09.

Malmqvist, M. (1978), Degradation of Agarose Gels and Solutions by Bacterial Agarase, *Carbohydrore Research* 62 (2), pp. 337–348, DOI: 10.1016/S0008-6215(00)80880-0.

Mikhailov, V. V., Romanenko, L. A., and Ivanova, E. P. (2006), The Genus *Alteromonas* and Related Proteobacteria, *Prokaryotes* 6, pp. 597–645, DOI: 10.1007/0-387-30746-x_20.

Miller, M. B. and Bassler, B. L. (2001), Quorum Sensing in Bacteria, *Annual Review of Microbiology* 55, pp. 165–199, DOI: 10.1146/annurev.micro.55.1.165.

Silhavy, T. J., Kahne, D., and Walker, S. (2010), The Bacterial Cell Envelope, *Cold Spring Harb. Perspect. Biol.* 2 (5), a000414, DOI: 10.1101/cshperspect.a000414.

Yates, G. T. and Smotzer, T. (2007), On the lag phase and initial decline of microbial growth curves, *Journal of Theoretical Biology* 244 (3), pp. 511–517, DOI: 10.1016/j.jtbi.2006.08.017.

7 Experimental method

7.1 Fabrication of microfluidic devices

Depending on the individual applications, the fabrication and treatment of microfluidic devices may vary significantly. In most cases the manufacturing steps include UV lithography and soft lithography (Figure 7.1). In UV lithography, the microfluidic patterns are developed on silicon wafers that are polymerized with SU-8 polymer. The subsequent step is soft lithography, which involves the fabrication of polydimethylsiloxane (PDMS) devices. PDMS is a transparent and viscous silicon-based polymer which has the characteristic that after curing it turns into an elastic solid. It is mixed with curing agent at a ratio of 10:1 and the mixture is degassed in vacuum. The mixture is then poured onto the SU-8 wafer and incubated at 80 ℃ for one hour. This way a copy of the channels pattern is created onto the PDMS layer. The PDMS slab is then bonded covalently on a 26 mm x 75 mm PDMS-covered glass slide, by exposure to oxygen plasma treatment (Figure 7.2). Finally, 3 mm x 5 mm inlet and outlet reservoirs are attached to the device.

In the current experiments agarose-in-oil emulsions are used for the synthesis of droplets. For this reason, after their fabrication, the droplet-based microfluidic devices undergo silanization using alkane silanes that turns their surface hydrophobic. This process involves the treatment of the PDMS devices with an anti-sticking reagent ([Tridecafluoro-1,1,2,2- tetrahydrooctyl] trichlorosilane) in a glove box. The synthesized particles are then run together with distilled water in a DLD device. After the oxygen plasma bonding, the hydrophilic DLD devices are treated with the anti-sticking 0.2 % poly-L-lysine–graft–polyethylene glycol (PLL-g-PEG) reagent. The analytical protocol for soft lithography and for the silanization treatment is

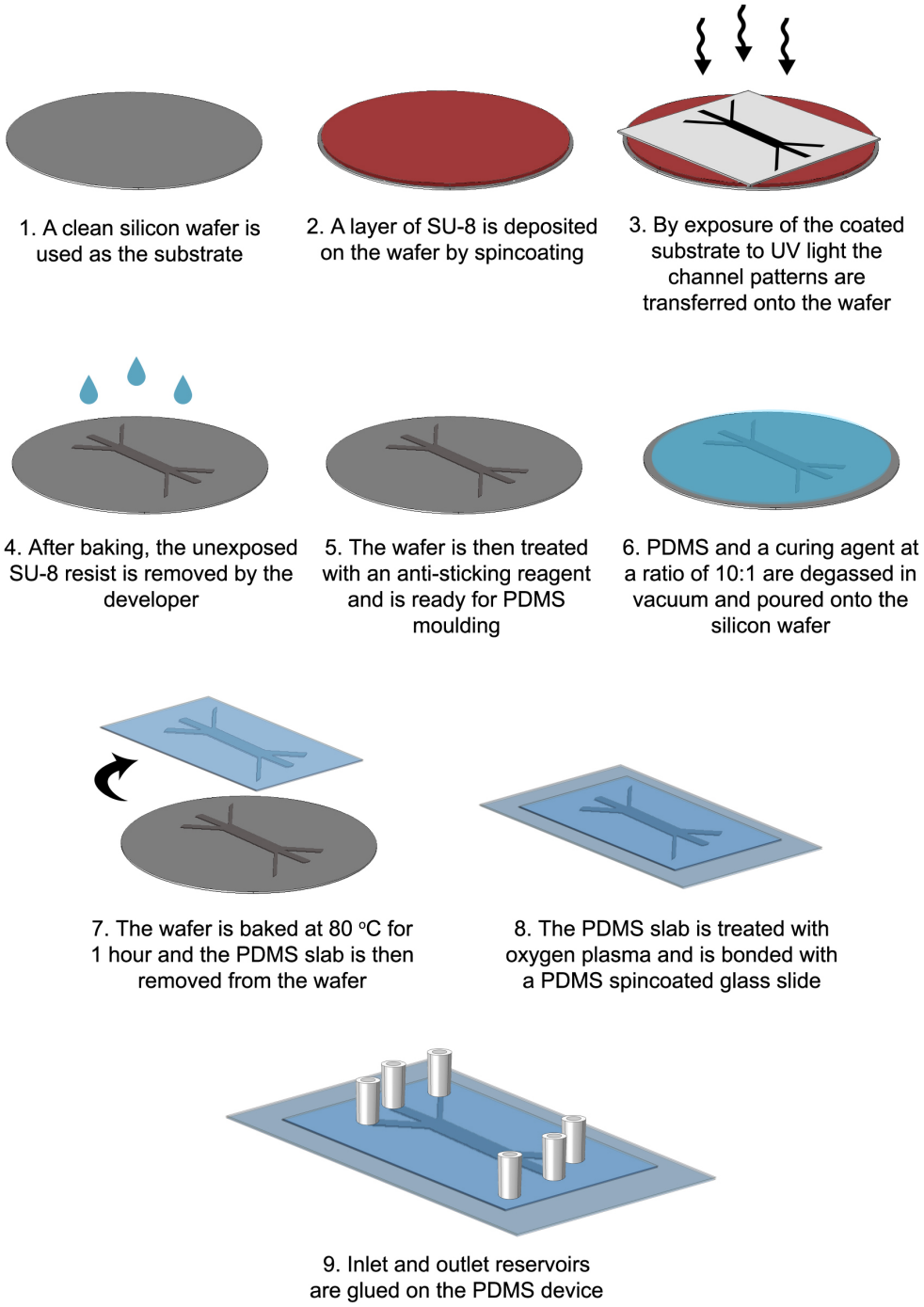

Figure 7.1: Illustration of UV- and soft- lithography. The fabrication of a patterned silicon wafer using UV lithography (1-5). The moulding of PDMS using soft lithography and the fabrication of a PDMS device (6-9).

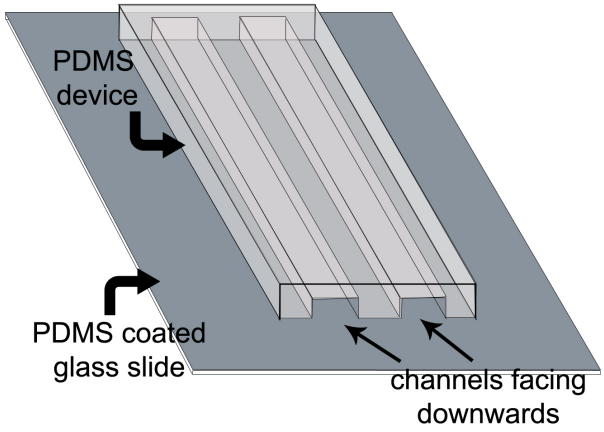

Figure 7.2: Illustration of the microfluidic channels of a PDMS device fabricated with soft lithography.

described in Appendix B.

7.2 Synthesis of agarose droplets

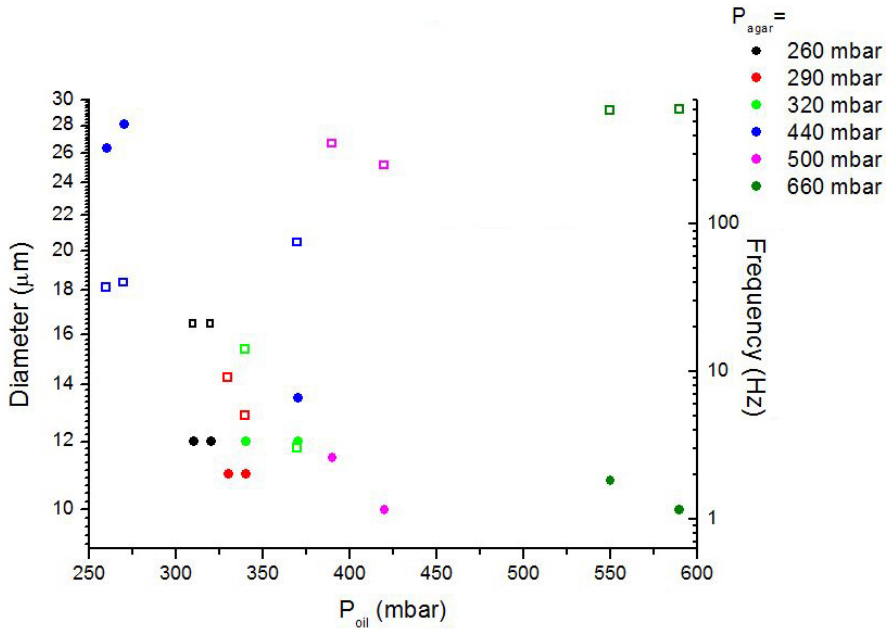

Figure 7.3: Generation frequency (□) and diameter (•) of the produced droplets as a function of the applied oil and agarose pressures.

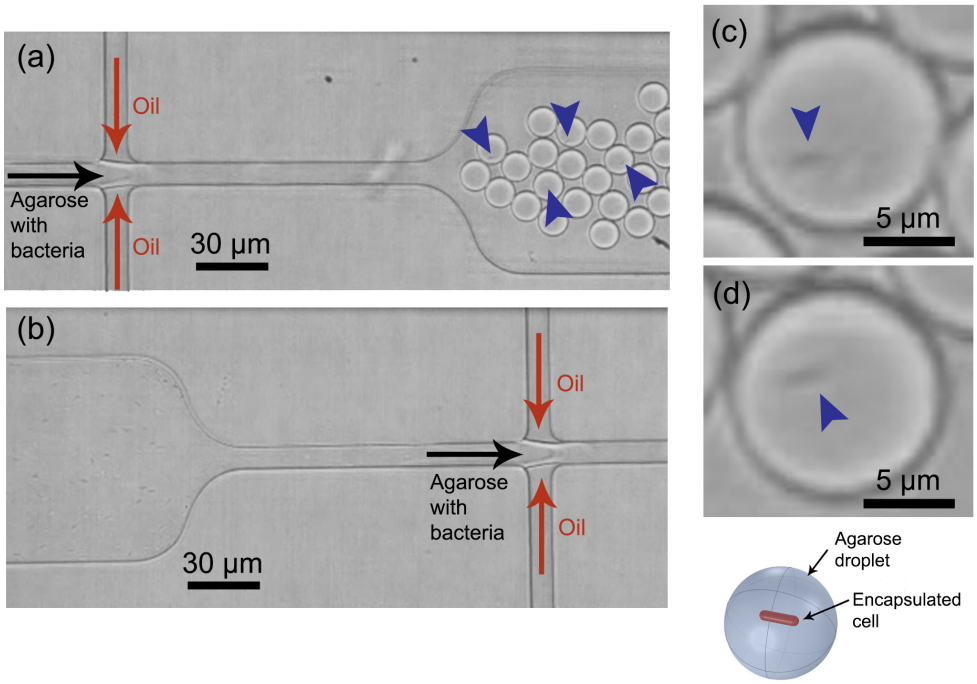

Figure 7.4: (a) A video-still of the generation of agarose droplets containing *Pseudomonas atlantica* bacteria as seen under the microscope with a 20x objective. The agarose pressure is 600 mbar and the oil pressure is 450 mbar. The diameter of the generated droplets is 12.5 μm and the generation frequency is 350 Hz. The most visible bacteria are indicated with blue arrows. In the captured videos bacteria are distinguished more easily due to their movement inside the droplets. (b) The bacteria suspended in the agarose solution as seen before the formation of droplets. (c),(d) A zoom-in at two droplets, each one containing a single bacterium.

For the preparation of the *Pseudoalteromonas atlantica* bacteria (strain AR06, isolated in Japan, 1987), the bacteria were initially grown on agar plates and then cultivated in Marine broth growth medium in a final concentration of 10^6 cells/mL. In order to examine the hydrolysis of agarose and thus identify the presence of secreted agarase enzymes, the bacteria were initially encapsulated into agarose droplets. Since *Pseudomonas atlantica* are quorum sensing bacteria, the secretion is initiated when they sense that the bacterial concentration in their environment is high. By encapsulating pairs of bacteria in a confined droplet volume of 0.5 pL, a high bacterial concentration is achieved. For the encapsulation, 3 μL of bacteria were diluted into 78 μL of 1% ULMP agarose gel in Marine broth medium. At this dilution the probability that pairs of bacteria are encapsulated is maximized. The solution was then run

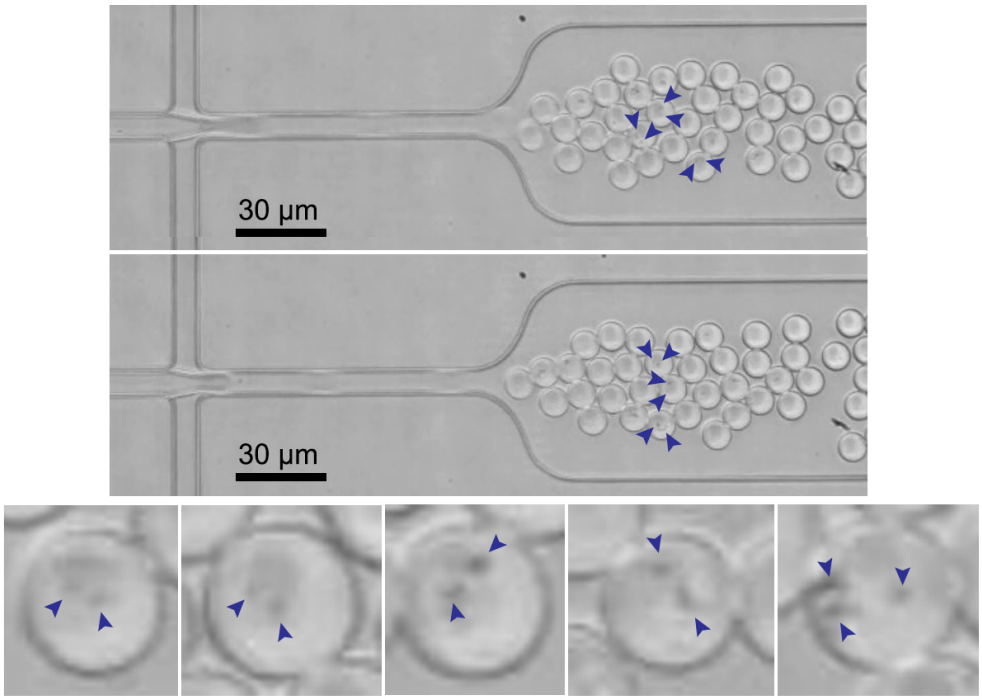

Figure 7.5: Video-stills of the generation of agarose droplets containing *Pseudomonas atlantica* bacteria. The agarose pressure is 600 mbar and the oil pressure is 590 mbar. The arrows indicate the bacteria inside the droplets. Pairs and triples of cells can be distinguished. The generation frequency is 500 Hz and all droplets have a diameter of approximately 10 μm.

in the flow-focusing device as the dispersed phase. Fluorinert® FC–40 oil containing surfactants was used as the continuous phase for the production of agarose droplets containing the bacteria. A high pressure regulator (Fluigent, maximum pressure 1000 mbar) was used to provide the pressure needed for the fluids to flow through the device.

The droplet sizes and the applied pressures had to be chosen so that the droplet generation frequency and the encapsulation rate of at least single cells would be maximized. Tests, where polystyrene fluorescent beads of 3 μm in diameter were encapsulated into agarose droplets, were run prior to the hydrolysis assay. These tests showed that the number of droplets containing single particles of 3 μm in size is maximized at a droplet diameter of approximately 11-12 μm. Figure 7.3 shows that for a droplet diameter of 11 μm the generation frequency of droplets increases at high oil and agarose pressures. Due to the mass conservation and for constant oil pressure we have $r^3 \cdot frequency \cdot P_{agar}^{-1} = constant$. The chosen pressures varied from 550

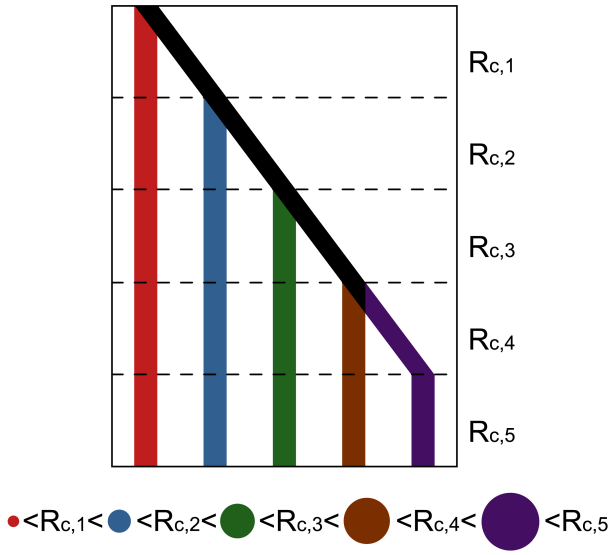

Figure 7.6: Separation of particles of several different sizes in a chirped DLD device, where the periodicity and therefore the critical radius of the device are successively altered.

mbar to 800 mbar for the agarose and from 450 mbar to 700 mbar for the oil.

Videos of the droplet formation and the bacteria encapsulation were recorded using an inverted fluorescence microscope (Nikon TE-2000U) and an EoSens® mini high speed camera (operating with MotionBLITZ® software) (Figures 7.4,7.5). The device was run for 4-5 hours and the volume of the generated sample was approximately 5 μL.

7.3 DLD experiments

The size range of the particles to be separated is an important factor that determines the final design of a DLD device, *i.e.* so that clogging of the device by too large particles can be avoided. Particles that appear to have a size larger than a critical size will be displaced and separated from seemingly smaller particles. However, in an array of a certain periodicity only binary separation can be achieved, meaning that there can only be separation between particles with smaller and larger sizes than the critical one. Nevertheless, there are many applications where a separation into multiple sizes is desired, for instance for separation of the components of whole

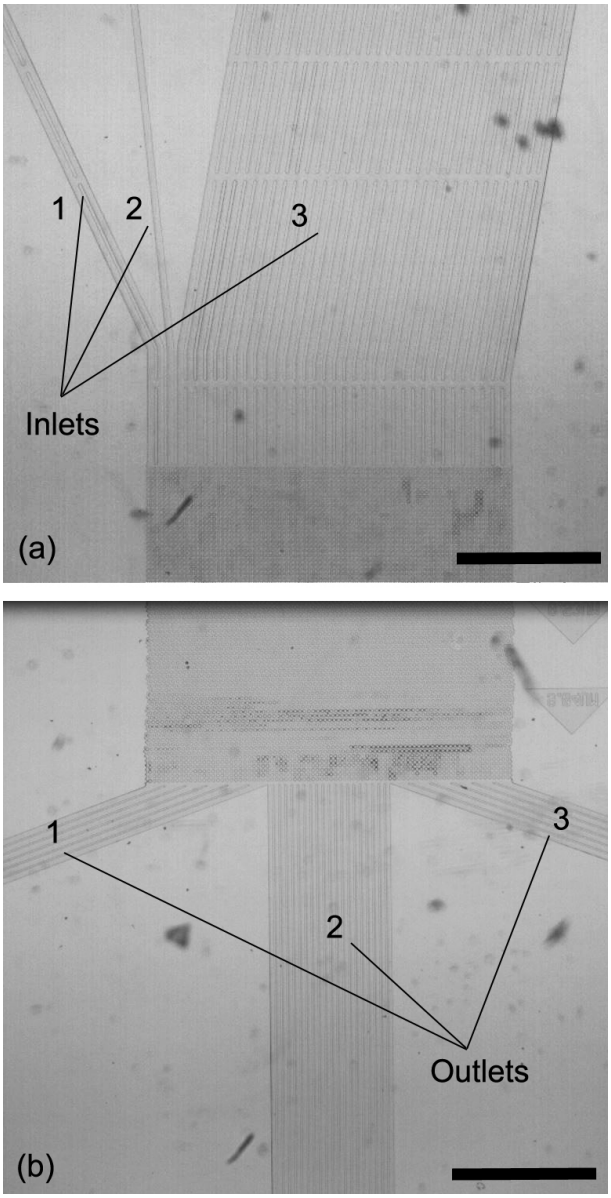

Figure 7.7: The three inlets (a) and outlets (b) of a DLD device for the injection and the collection of the different reagents respectively. Image taken using a 2x magnification. Scale bars are 1 mm.

blood (Davis *et al.*, 2006).

This can be achieved in a so called chirped device. Such a device consists of an array that has a successive change in its periodicity by altering the center-to-center post distance λ or the relative shift of two subsequent rows

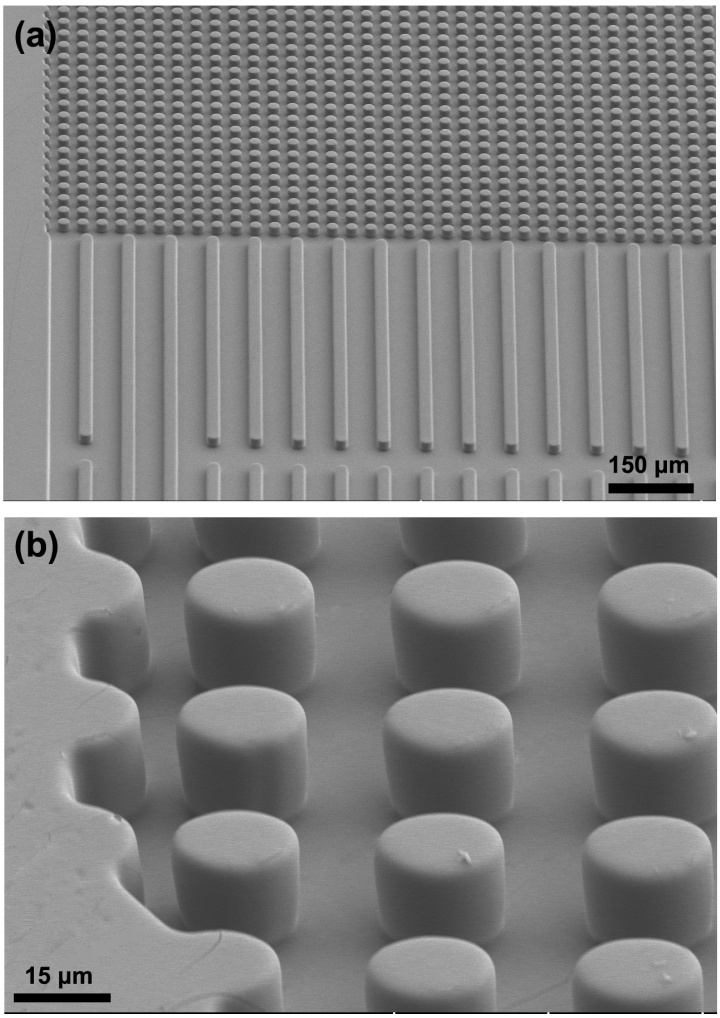

Figure 7.8: SEM images of the entrance (a) and the posts (b) of the DLD device.

of posts $\Delta\lambda$. According to equation 3.4 a change in the periodicity, but also in the post diameter, results in a change in the critical radius. Thus, by successively changing the critical radius in a single DLD device, spatial separation of particles with a broad range of sizes can be achieved, see Figure 7.6. Usually the critical size increases as the periodicity is successively changed, however devices where the critical size decreases can also be designed (Holm, 2012).

For the injection of a sample into the device and also for the collection after the different components have been separated, the main array is connected to inlet and outlet reservoirs via channels. Usually DLD devices consist of

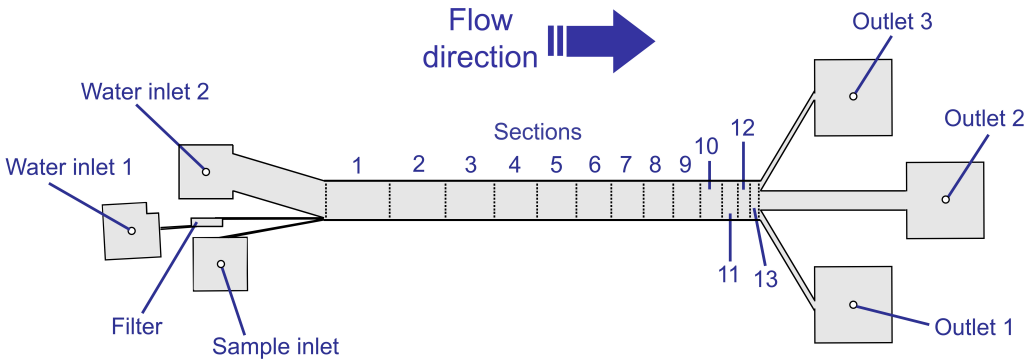

Figure 7.9: A DLD device that consists of 13 sections, each one corresponding to a different periodicity. Each section with a certain critical radius consists of a number of repeated regions with the same characteristics. The droplet sample is injected in the first side inlet, while water is injected in the middle and the second side- inlets. After the separation in the device, the droplets are collected from the three outlets of the device.

multiple inlets, each one being used for injection of a different reagent like e.g. the sample or buffers. In Figure 7.7a the three inlets of a typical DLD device are illustrated. The side- inlets (inlets 1 and 3 as shown in Figure7.7a) are used for injection of reagents. The inlet in the middle is used for the injection of the sample. In order to ensure that the injected sample is filtered before entering the device, the channel also consists of a filter where large particles are removed to reduce clogging in the separation array. Similarly to the inlets, the outlets of the device consist of channels that connect the main array with the outlet reservoirs, see Figure 7.7b. All DLD devices consist of multiple outlets, so that the separated components of the sample can exit the device and be collected at different points. In Figure 7.8 an SEM image of the entrance and the posts of the device is also shown.

The DLD devices used in the current project were chosen according to the size range of the particles to be sorted. The sizes of the synthesized droplets lie within the range of 8 μm to 10 μm. The characteristics of the used devices are listed in Table A.1 in the Appendix. The periodicity N of the array was successively decreased by increases in the relative shift of the post rows, $\Delta\lambda$, whereas the gap between the posts, d, was kept constant throughout the device.

Figure 7.9 illustrates a device that consists of 13 sections. Each section of the array with a certain critical size consists of repeated regions, all having the same characteristics. The number of repeats depends on the size range

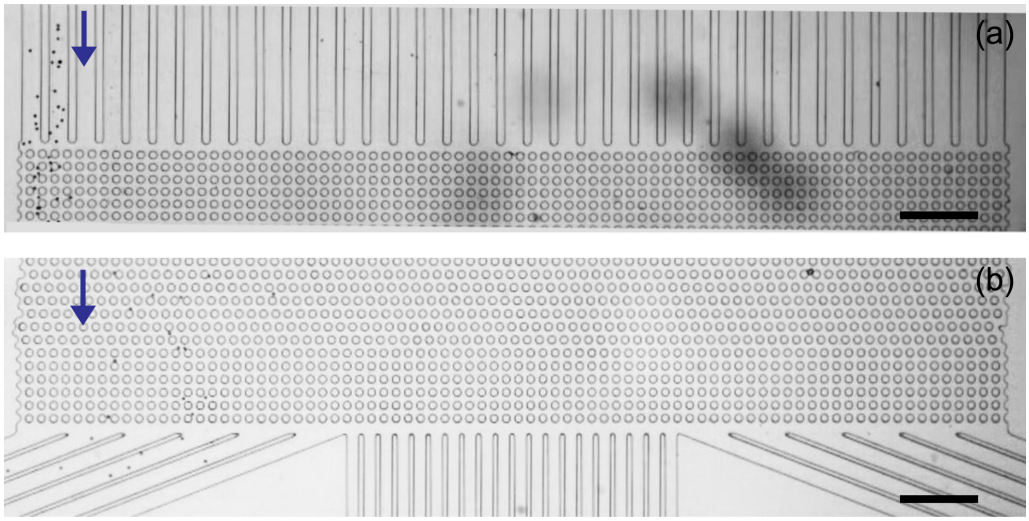

Figure 7.10: Video-stills of the droplets (a) entering and (b) exiting the DLD device as seen with a 4x objective at 600 mbar. The arrows indicate the direction of the flow. The scale bars are 200 μm.

of the particles to be separated. In the current design each section consists of five repeats. The net effect of the particles' motion in each of these sections is a spatial separation of high throughput and high resolution. A particle larger than the critical size is laterally displaced by a distance equal to the center-to-center post distance λ when they exit the first region. After having travelled through the whole section, the particle is displaced by a lateral distance of approximately 5λ. It is therefore possible, by knowing in advance the sizes of the particles to be separated as well as the device characteristics, to predict the behaviours of the particles in the device (Holm, 2012).

The length of the main array is approximately 27 mm and the depth of the device is 17 μm. The device consists of three inlets for injection of the reagents and three outlets for collection of the particles. Details on the geometry of the DLD device are presented in Appendix A. The synthesized droplet particles were injected in the first side- inlet (see Figure 7.9), in order to prevent the droplets from being filtered in the middle inlet. Distilled water was injected in the middle and the second side- inlets.

After the completion of the encapsulation experiments, the agarose droplets were kept in the oil phase overnight (~ 16 hours). They were then extracted from the oil using 1H,1H,2H,2H–Perfluorooctanol and suspended in distilled water. After injection in the DLD device, the sample was allowed to flow

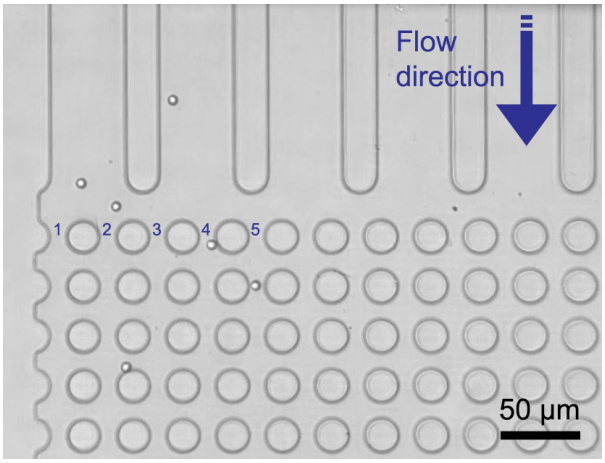

Figure 7.11: Video-still of the droplets entering the DLD device as seen with a 20x objective at 100 mbar. The numbers indicate the entrance gaps for the droplets.

through the device together with water. However, the contrast of the agarose droplets when run in water was very low due to the similar refractive index of the water and the droplets.

For this reason generated droplets that contained *Pseudomonas atlantica* bacteria were initially incubated at room temperature and then run with Fluorinert® FC–40 oil in a silanized DLD device. In this case the difference between the refractive index of the droplets and that of the oil resulted in an increased contrast for the agarose droplets. As a negative control for the deformation of *Pseudomonas atlantica*-containing droplets, *Bacillus subtilis* bacteria that do not secrete agarase were also encapsulated. They are rod-shaped bacteria with dimensions and concentration similar to those of the *Pseudomonsd atlantica* (see Appendix D for the cultivation protocol). The pressure difference across the device was applied using the pressure regulator. Nine different pressure values were applied during the experiment: 50, 100, 200, 300, 400, 500, 600, 700 and 800 mbar. Videos were recorded at the entrance and the outlets of the device using the high speed camera (Figures 7.10, 7.11). The duration and the frame rate of the captured videos varied, from 30 to 90 seconds and from 50 to 800 frames per second, depending on the applied pressure. The captured videos at the outlets of the device were analyzed in order to examine the distribution of the droplets when exiting the device. According to the physical model presented in section 3.2.2 however and as it will be later discussed in section 8.3, agarose droplets that are suspended in oil cannot deform easily due to the interfacial energy that

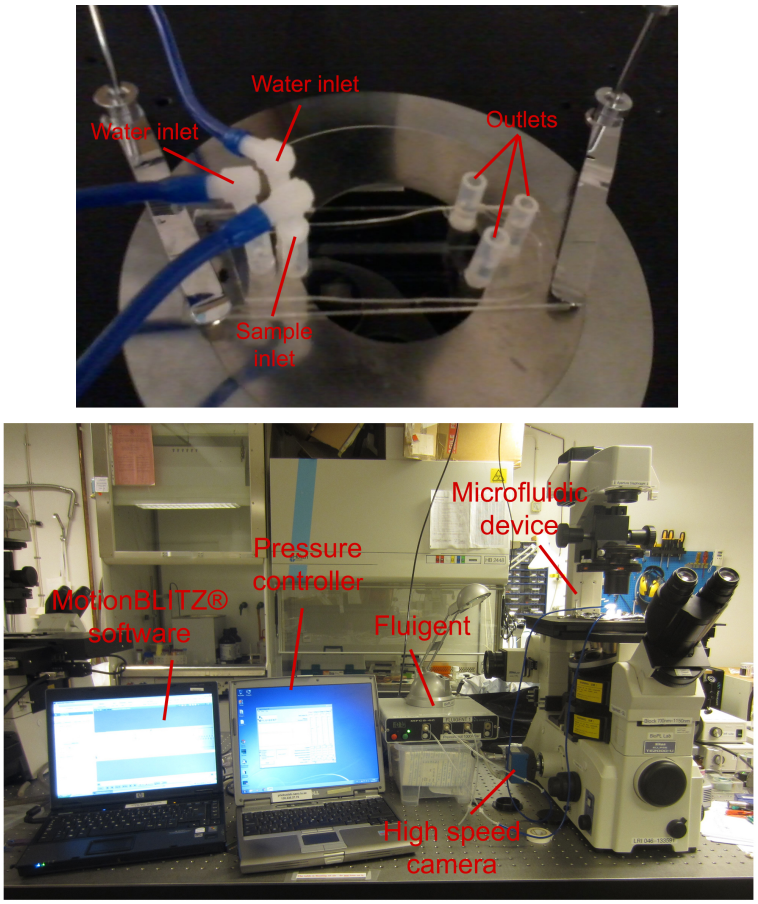

Figure 7.12: Image of a DLD device and the setup where the experiments were performed.

resists deformation.

Thus the experiments, where samples with the two bacterial types were examined, were repeated in water. The droplets were initially incubated into the oil overnight at 35 ℃ in order to allow the secreted agarase to diffuse away from the bacteria and hydrolyze the agarose. After incubation the drops were left 30 minutes at room temperature to cool. For extracting the samples from the oil phase, 1H,1H,2H,2H–Perfluorooctanol was used and the droplets were then diluted in distilled water at a ratio of 1:6. Following this they were centrifuged at 20 g for an increased concentration and then were run in the DLD device. As an additional test, agarose droplets containing 2.1 μm sized fluorescent polystyrene beads were synthesized and were also run in DLD devices. In Figure 7.12 a DLD device and the setup of the experiments are shown.

References

Davis, J. A., Inglis, D. W., Morton, K. J., Lawrence, D. A., Huang, L. R., Chou, S. Y., Sturm, J. C., and Austin, R. H. (2006), Deterministic hydrodynamics: Taking blood apart, *PNAS* 103 (40), pp. 14779–14784, DOI: 10.1073/pnas.0605967103.

Holm, S. H. (2012), Microfluidic Cell Sorting and Analysis – Point-of-Care Diagnosis of Human African Trypanosomiasis, Master Thesis, Lund: Lund University.

8 Results and discussion

8.1 Bulk agarose hydrolysis assay

Prior to the examination of the degradation of agarose gels by β-agarase secreted by the *Pseudoalteromonas atlantica* bacteria, agarose hydrolysis by pure β-agarase (Sigma Aldrich, specific activity ≥5,000 units/mg protein) was tested. Two different concentrations of β-agarase in PBS (Phosphate Buffered Saline), 10 units/mL and 50 units/mL, were initially mixed with 1% ULMP agarose gel in water and incubated for one hour at approximately 40 ℃. The mixtures were then allowed to cool down for approximately 20 minutes and inspected for digestion of agarose (Shoichet *et al.*, 1996; Ng *et al.*, 2009). The digestion of the agarose gel was indicated by its liquefaction. The results were then compared with a blank sample that was used as reference.

No liquefaction was observed for the latter. The assay was then repeated by injection of the same enzyme concentrations into 1% of hardened ULMP agarose, without an incubation step and results similar to the ones from the first assay were obtained. These experiments were performed in order to verify the effect of the enzyme on the agarose gel and the results showed that hydrolysis, thus softening of the gel is possible. The analytical protocols for the agarase hydrolysis assay by pure β-agarase are described in Appendix C.

8.2 Encapsulation of bacteria in agarose droplets

The suspension of the bacteria in the agarose solution prior to the encapsulation experiment (at the ratio 3:78) yielded a high probability of encapsulation of multiple bacteria per drop ($P = 51\%$), whereas the probability that a drop

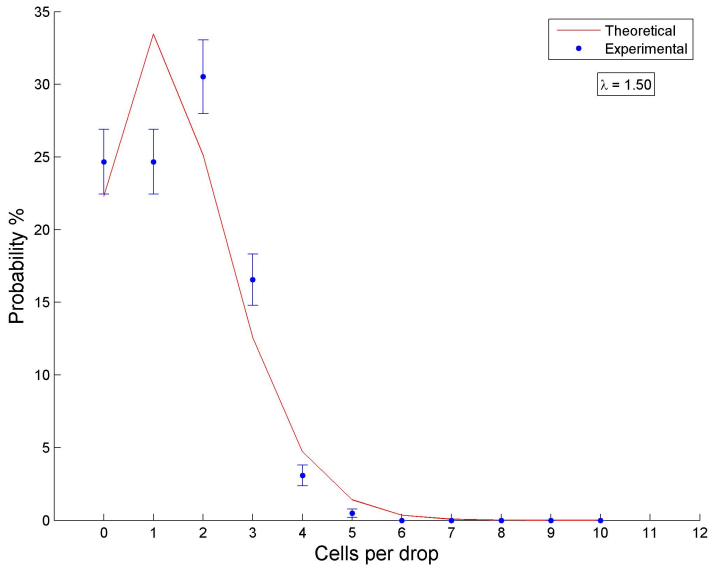

Figure 8.1: Probability distribution for the number of encapsulated bacteria per droplet during the synthesis of the particles.

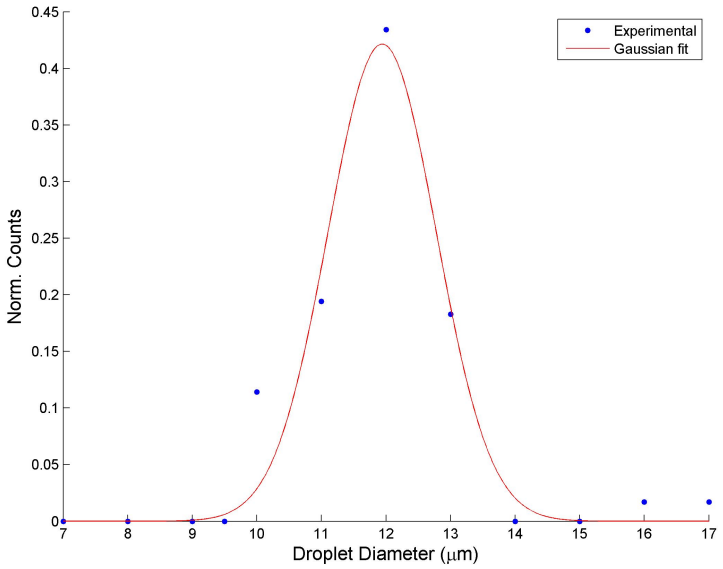

Figure 8.2: Droplet size distribution, prior to the incubation step, for droplets with *Pseudomonas atlantica* bacteria that were later run in a DLD device with water.

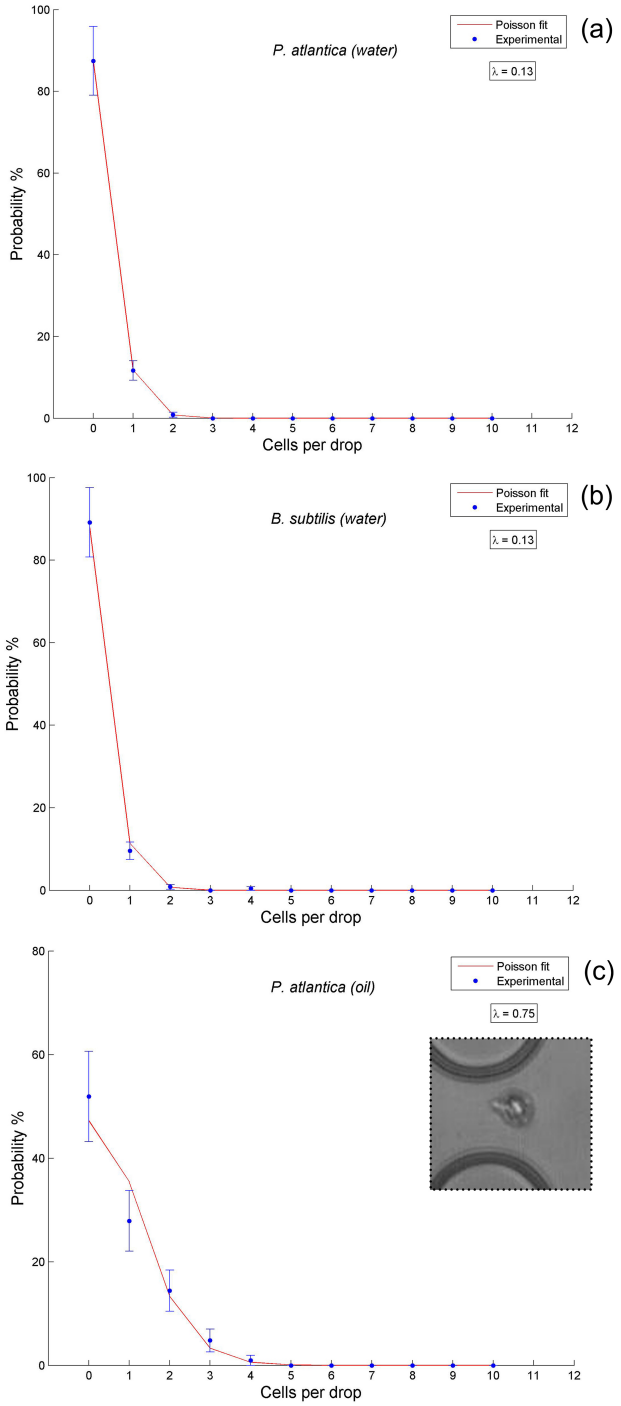

Figure 8.3: Probability distributions for the number of encapsulated cells per droplet after the incubation of the *Pseudomonas atlantica*-containing sample in water (a), the *Bacillus subtilis*-containing sample in water (b) and the *Pseudomonas atlantica*-containing sample in oil (c). The inset in (c) shows a bacterium that is possibly trapped at the interface of the droplet with the oil.

would contain no bacteria was lower ($P = 23\%$). The experimentally determined distribution for the number of bacteria encapsulated per drop before the incubation is shown in Figure 8.1 and is in agreement with the theoretical Poisson distribution for the same average number of cells per drop, $\lambda = 1.50$. Figure 8.2 shows the size distribution of generated droplets containing *Pseudomonas atlantica* bacteria. The droplet diameters are in a good agreement with a normal distribution with a mean droplet diameter of (12 ± 1) μm.

Figure 8.3 shows the probability distributions for the number of encapsulated cells per droplet after the incubation of the samples and prior to their sorting. The number of cells per droplet for both *Pseudomonas atlantica*- and *Bacillus subtilis*-containing droplets that were run in water shows a notable decrease ($\lambda = 0.13$) compared to the initial average number of cells per drop ($\lambda = 1.50$). These results indicate that in both cases a number of encapsulated bacteria have escaped the droplets, a fact that will be considered in section 8.4.

It has been observed that after the gelification of an agarose solution prepared with water, a thin layer of water remains on the surface of the gel. This thin layer is probably released when the polymeric network is formed. Thus, bacteria that might be at the interface of the droplet with the oil during the synthesis of the particles, could escape the droplet together with the released water. As previously mentioned these droplet samples, prior to the DLD experiments, were also incubated at 35 ℃ and then suspended in water and centrifuged. At this temperature however, the agarose droplets can soften due to the gelation hysteresis effect. This might result in the escape of the cells from the droplets. Another reason for their reduced number per droplet could also be the centrifugation of the sample. During centrifugation, the gelified droplets could break, resulting in bacteria free in the solution. Finally, the index of refraction of the droplets might be affected by the gelification of the agarose. This might also make it more difficult in some cases to distinguish the cells inside the droplets.

On the contrary *Pseudomonas atlantica*-containing droplets that were run in oil show a smaller decrease of the average number of cells per drop ($\lambda = 0.75$) compared to the initial ($\lambda = 1.50$). Fewer bacteria were observed free in solution, as in this case the sample was incubated at room temperature and without a centrifugation step. In addition, the sample was kept in the oil throughout the whole experiment. Therefore the bacteria could also remain trapped at the interface of the droplets with the oil (see inset in Figure 8.3c). The observed decrease of the number of cells per droplet could also arise from

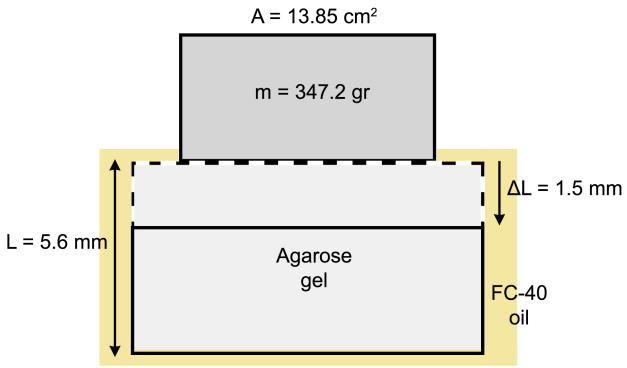

Figure 8.4: Deformation of a bulk agarose gel that is surrounded by FC-40 oil, by a weight m.

the change in the index of refraction of the agarose.

8.3 Deformation of droplets

The experimentally obtained values of the maximum flow velocity and the shear rate from the captured videos at 100 mbar and 600 mbar for Fluorinert® FC–40 oil were $v = (1.1 \pm 0.6)$ mm/s, $\dot{\gamma} = (3.6 \cdot 10^2 \pm 1.9 \cdot 10^2)$ s^{-1} and $v = (4.6 \pm 2.1)$ mm/s, $\dot{\gamma} = (1.5 \cdot 10^3 \pm 0.7 \cdot 10^3)$ s^{-1} respectively. From the experimentally obtained shear strain rate values in oil and according to the deformation model described in section 3.2.2, we obtain the shear force that is applied on the droplets due to the interaction with the posts in the DLD device. For a maximum deformation of a bulk agarose gel surrounded by FC-40 oil, $\Delta L = 1.5$ mm (Figure 8.4), we obtain the Young's modulus and the spring constant:

$$Y = \frac{\sigma}{\epsilon} \simeq 10\,\text{kPa} \quad \text{and} \quad k = \frac{mg}{\Delta L} \simeq 2.3 \cdot 10^3\,\text{N/m} \tag{8.1}$$

Assuming a relaxation time of approximately $\tau \simeq 10$ ms and since $\tau = \mu A/kL$ we obtain the viscosity of the agarose gel, $\mu \simeq 90$ Pa·s. Thus, from equation 3.15 we can calculate the exerted shear force at different shear rates. At the pressure of 600 mbar, $\dot{\gamma} \simeq 1.5 \cdot 10^3$ s^{-1} and for a droplet radius of $r = 5$ μm, we obtain $F_{600} \simeq 22$ μN. Similarly at a flow pressure of 100 mbar we obtain $F_{100} \simeq 5.2$ μN. By comparing the experimentally obtained forces with the ones that are theoretically required to induce a droplet deformation (Figure 3.10) one can see that the shear forces in the hydrophobic DLD would be sufficient to induce deformations of up to 40 μm, meaning a relatively strong

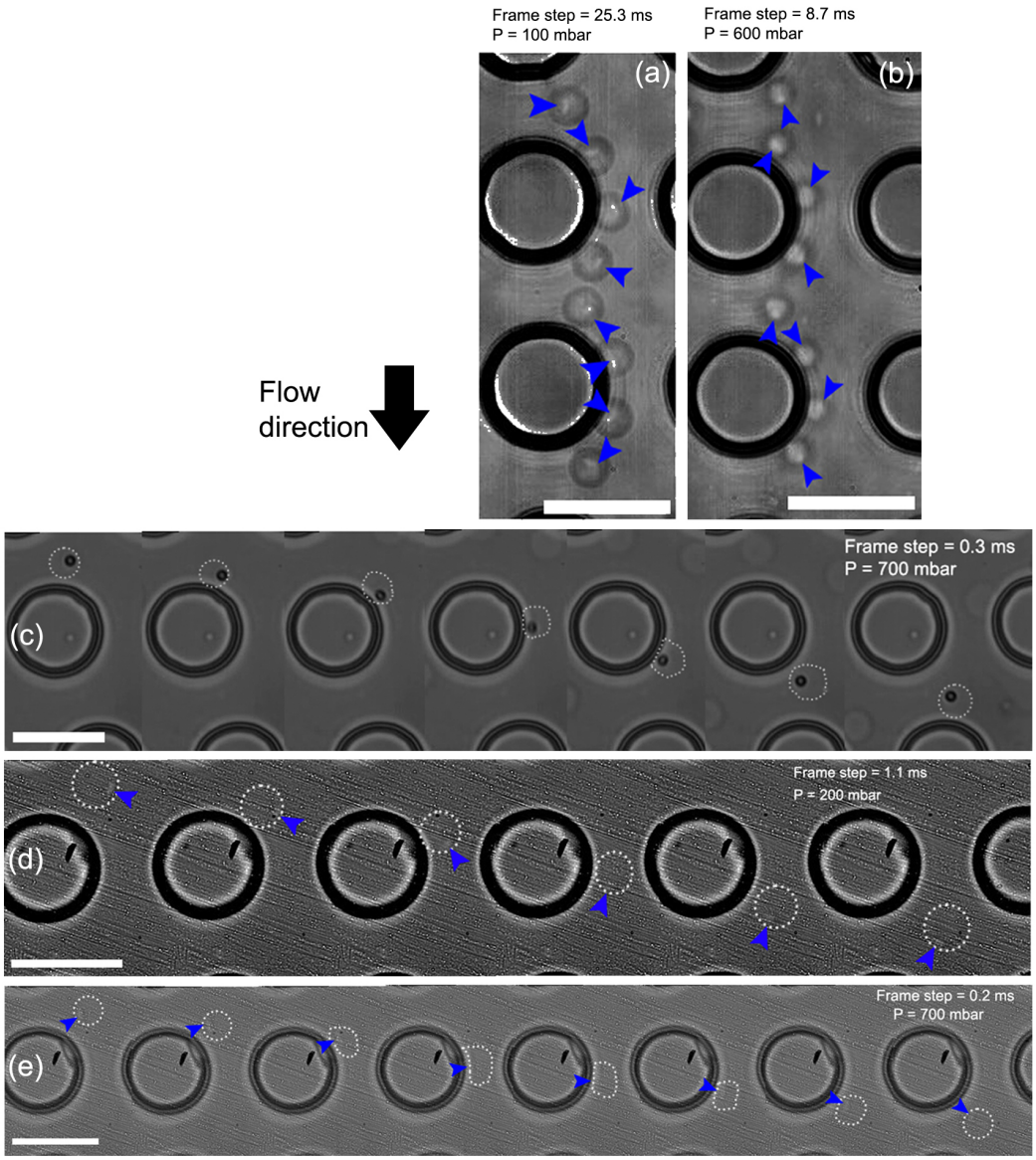

Figure 8.5: Video frames showing the behaviour of the droplets close to a post in the DLD device, taken with a 60x water objective. Droplets containing *Pseudomonas atlantica* bacteria that were run in oil at 100 mbar (a) and 600 mbar (b). A droplet in water that contains a polystyrene bead at 700 mbar (c). Droplets containing *Pseudomonas atlantica* bacteria that were run in water at 200 mbar (d) and 700 mbar (e). The arrows indicate the positions of the bacteria inside the droplets. The droplets in (c), (d) and (e) are highlighted for better visualization. Scale bars are 20 μm.

Table 8.1: Mean droplet diameters for the different samples during the generation of the particles and after their incubation overnight. The errors correspond to the standard deviations of the normal size distributions.

	Diameter at generation (μm)	**Diameter after incubation (μm)**
***P. atlantica* (water)**	11.8 ± 1.3	8.9 ± 0.4
***B. subtilis* (water)**	11.4 ± 0.9	8.5 ± 0.6
***P. atlantica* (oil)**	11.6 ± 1.9	8.7 ± 2.3
***B. subtilis* (oil)**	11.4 ± 2.0	8.4 ± 1.3
Polystyrene beads (water)	10.1 ± 0.5	8.4 ± 0.5

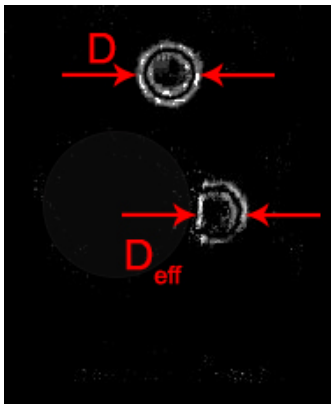

Figure 8.6: The software ImageJ was used to analyse the videos and to measure the initial size of the droplets (D) and their effective size (D_{eff}).

force. In the theoretical model however the deformation of water droplets (instead of agarose droplets) in oil is estimated. It is thus expected that agarose droplets will be deformed less by the relevant forces in the DLD, due to the increased stiffness of the agarose gel. The results for the deformation of the agarose droplets are discussed later in this section.

In Figure 8.5 the behaviour of the different agarose droplets encountering a post in a DLD device is shown. When the droplets that contain *Pseudomonas atlantica* bacteria are run in oil, the deformation is not significant both at low and at high pressures, due to the surface tension that resists the deformation (Figures 8.5a-b). Droplets that contain polystyrene beads exhibited a similar behaviour at high pressures when run in water, as in this case no enzyme is present in the solution; thus the agarose is not hydrolyzed (Figure 8.5c). On the contrary high pressures, thus higher shear rates, result in a larger deformation of *Pseudomonas atlantica*-containing droplets in wa-

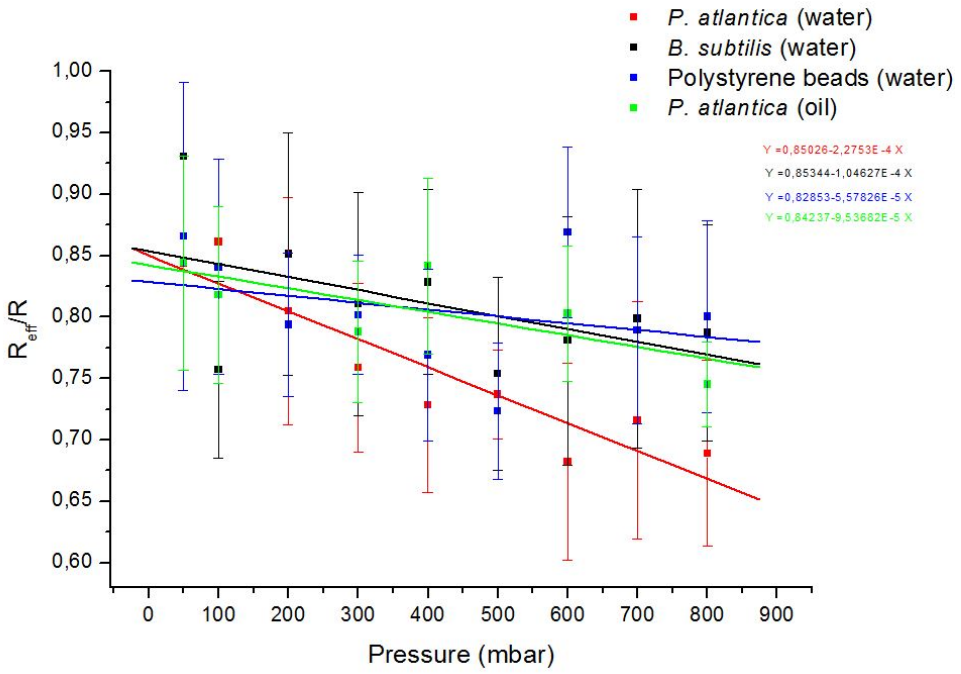

Figure 8.7: Results from the direct measurements of the initial and the effective sizes of the droplets. The mean ratio of the effective size of the different droplet samples to their initial size is plotted against the applied pressures. The error bars correspond to the standard deviation of the ratio distribution at each pressure. Linear fits are also made to quantitatively compare the results.

ter, compared to their deformation at lower pressures (Figures 8.5d-e). This is due to the fact that at the pressure of 700 mbar, the deformable droplets are "squeezed" by the high shear forces and thus exhibit a smaller effective size in comparison to the one at 200 mbar.

As shown in Table 8.1 the sizes of the droplets during their fabrication varied from 10-12 μm in diameter. During their incubation overnight however, prior to the DLD experiments, the agarose droplets shrank down to 8-10 μm due to the evaporation of water. The high standard deviations for the samples in oil and the *Bacillus subtilis*-containing droplets in water indicate a heterogeneity in the droplets' sizes due to instabilities during their synthesis.

The deformation of the agarose droplets was quantitatively estimated by analysing the recorded videos with the image processing software ImageJ. The ratio of the effective size of the droplets to their initial size was measured as shown in Figure 8.6 and plotted against the applied pressure in

Figure 8.7. Due to technical problems with the high speed camera however, no videos at high frame rate were recorded for the *Bacillus subtilis*-containing droplets in oil, thus the examination of the deformation of the sample was not possible. The plotted ratio points correspond to the mean value of twenty data points and the estimated errors correspond to the standard deviations of the Gaussian distributions. By looking at the R_{eff}/R ratio, the variations in the initial size of the droplets are eliminated as only their relative deformation is examined.

By making a linear fit we can see that in all cases, an increase in the applied pressure results in a decrease of the R_{eff}/R ratio. At low pressures all droplets exhibit a similar degree of deformation. At 50 mbar the effective radii are approximately 84% of the initial radii of the droplets. As the pressure increases, the droplets containing the non-secreting bacteria *Bacillus subtilis*, the ones with polystyrene beads, as well as those with *Pseudomonas atlantica* that are run in oil, are slightly deformed in a similar way. However as the pressure increases, the R_{eff} of the *Pseudomonas atlantica*-containing droplets that are run in water decreases more.

As explained above, the slight decrease of the R_{eff}/R ratio for the droplets in oil and the droplets that do not contain *Pseudomonas atlantica* bacteria could be explained by the viscoelastic properties of the agarose. For the droplets that contained *Pseudomonas atlantica* and that were run in oil, deformations of 1.6 and 1.8 μm were observed at 100 and 600 mbar respectively. By considering the previously calculated forces that are exerted by the posts on the agarose droplets at these pressures, we obtain $k = (7.5 \pm 4)$ N/m, $Y = (2.4 \cdot 10^2 \pm 1.3 \cdot 10^2)$ kPa. As expected the stiffness of agarose gel droplets in oil appears to be larger compared to the theoretical stiffness of water droplets in oil with the same size ($k \simeq 0.5$ N/m, $Y \simeq 1.6 \cdot 10^2$ kPa). In a study from Stolz *et al.* (2004) the stiffness of 0.75% micrometer-sized agarose gels in water is found to be $k \simeq 0.4$ N/m, $Y \simeq 0.3 \cdot 10^2$ kPa. Since *Pseudomonas atlantica* bacteria are contained in the experimental samples, one would expect that the droplets would be softer due to hydrolysis. Nevertheless, compared to the typical stiffness of agarose gels in the microscale measured by Stolz *et al.* (2004), the gel droplets in oil appear to be slightly stiffer. Finally, the difference in the calculated spring constant of the agarose gel droplets in oil from that of the bulk agarose gel in oil (equation 8.1) is probably a result of the scaling of the examined system. For three-dimensional elastic objects, the scaling of the spring constant is proportional to the scaling of the ratio *cross section/length* of the object.

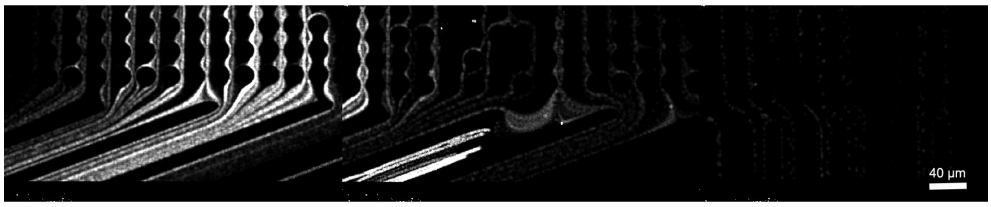

Figure 8.8: The trajectories of the droplets when exiting the device, thus their distributions, were obtained by removing the background of the recorded videos and overlaying the frames with the software ImageJ.

For droplets that contain the secreting bacteria however and that are run in water, a stronger dependence of the R_{eff}/R ratio on the pressure is observed. This is a first indication that these droplets have a higher degree of deformabiliy compared to the rest of the samples. Thus, as expected, the droplets with the *Pseudomonas atlantica* bacteria tend to be softer, possibly due to the hydrolysis of the agarose by the secreted enzyme. In addition, the effect of the medium can be seen, as unlike the droplets in oil, in this case there is no resistance from the water for the deformation of the droplets.

8.4 Sorting of agarose droplets in the DLD device

The differences in the deformability of the droplets were also examined by looking at the distribution of the particles when they exit the DLD device. In order to do that, the recorded videos at the exits of the device were analyzed with the ImageJ software.

The trajectories of the particles were acquired by removing the background and overlaying all the frames as shown in Figure 8.8. When run in the DLD device, the droplets enter the array from the gaps number 1-5 (Figure 7.11). Therefore, droplets that exit from gap number ~4 are considered to have zero displacement. As mentioned in section 7.3 a particle that has a size larger than the critical radius of a section in the DLD device, will be displaced by $5\lambda = 160$ μm after having travelled through the whole section.

In order to obtain the distribution near the outlets, the normalized intensities of particle trajectories were plotted against the lateral displacement for selected pressure values. The intensity values were obtained using the ImageJ software and were then normalized by the total intensity for each

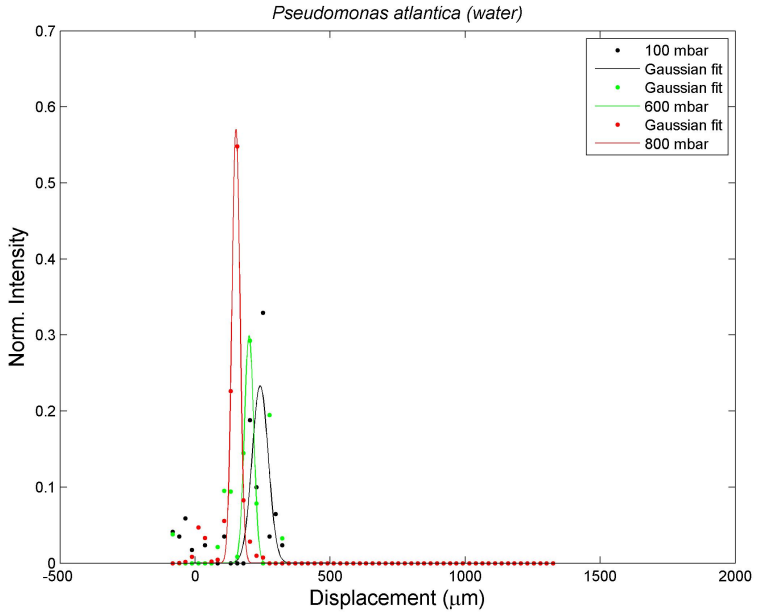

Figure 8.9: The binned lateral displacements of *Pseudomonas atlantica*-containing droplets in water at 100, 600 and 800 mbar.

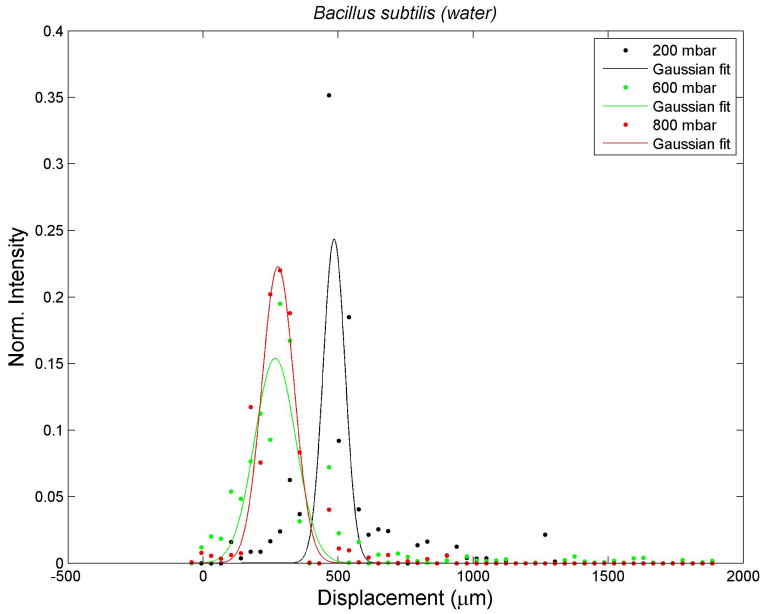

Figure 8.10: The binned lateral displacements of *Bacillus subtilis*-containing droplets in water at 200, 600 and 800 mbar.

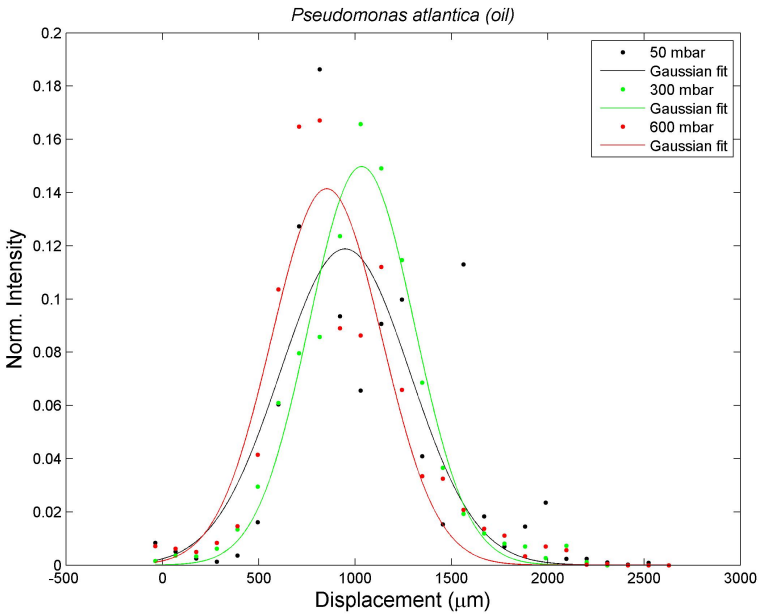

Figure 8.11: The binned lateral displacements of *Pseudomonas atlantica*-containing droplets in oil at 50, 300 and 600 mbar.

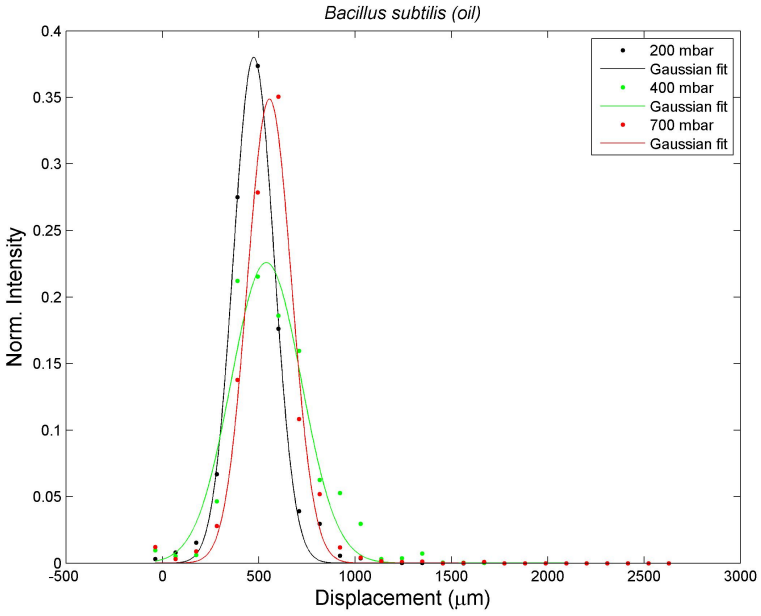

Figure 8.12: The binned lateral displacements of *Bacillus subtilis*-containing droplets in oil at 200, 400 and 700 mbar.

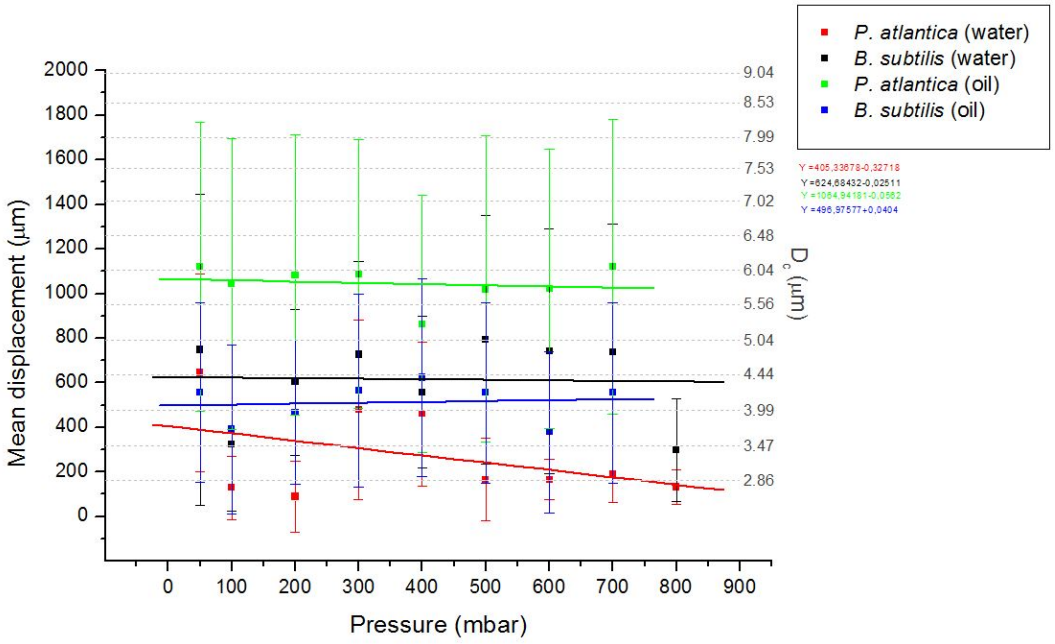

Figure 8.13: The mean displacements of the different droplet samples with varying pressure. The error bars correspond to the standard deviation of the displacement distributions at each pressure. Linear fits are also made to quantitatively compare the results. The corresponding theoretical critical diameters of the device D_c are also shown.

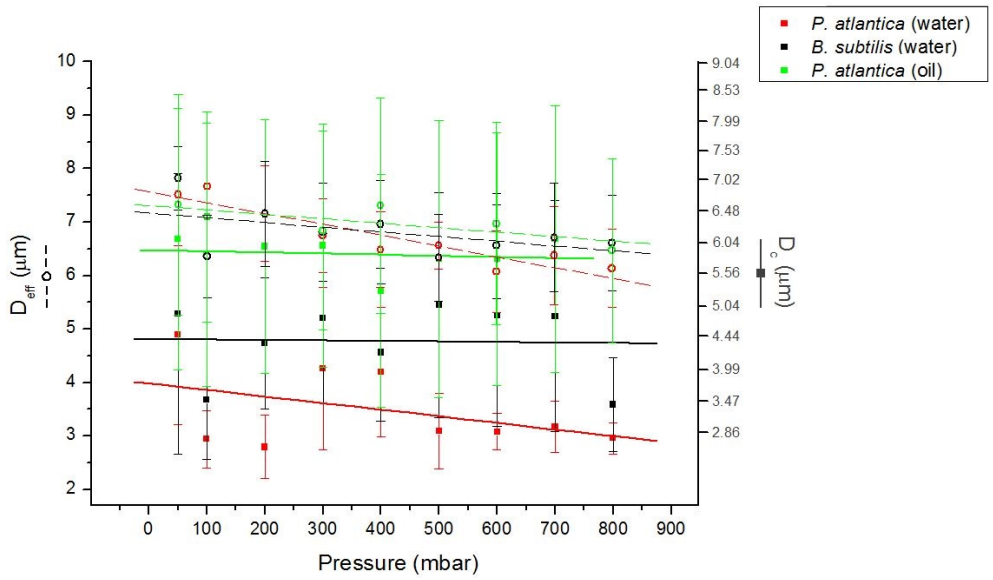

Figure 8.14: The calculated absolute effective sizes of the droplets as a function of the applied pressures. The resulting theoretical diameters of the droplets are also shown. Linear fits to the mean effective sizes (dashed lines) and to the mean theoretical sizes (solid lines) are made to quantitatively compare the results.

pressure and by the duration of each video. In order to reduce the effect of zero intensities at the positions of the array posts as well as the noise in the data, the values for the lateral displacement were binned. For each bin, the sum of the normalized intensities is plotted against the mean displacement of that interval (Figures 8.9–8.12). The lateral displacements are in a good agreement with a normal distribution. Due to clogging of the DLD device however, the examination of the distribution of droplets containing polystyrene beads was not feasible. In the case of the droplet samples that were run in water, small peaks at around zero displacement are observed. These peaks correspond to free bacteria in the solution and small debris as will be later discussed.

Figure 8.13 summarizes the displacements for all the different samples with varying pressure. The mean displacement for each distribution is plotted against the applied pressures. The corresponding theoretical critical diameters of the device D_c are also presented.

As a first observation, the results indicate a tendency of the mean displacement of *Pseudomonas atlantica*-containing droplets in water to decrease with increasing pressure. On the other hand *Bacillus subtilis*-containing droplets

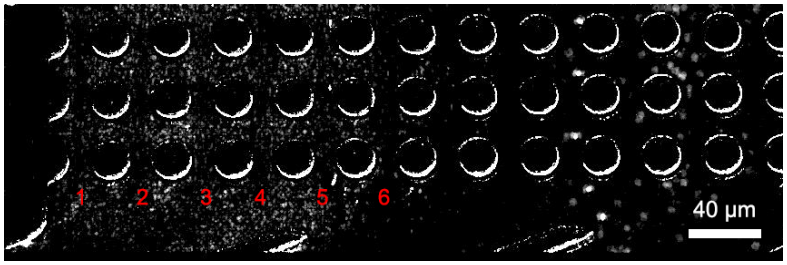

Figure 8.15: A frame overlay of *Pseudomonas atlantica*-containing droplets that are run in water at 200 mbar. Bacteria that are free in the solution flow in a "zig-zag" motion and exit the device from the first six post gaps.

in water as well as the samples that were run in oil show a smaller dependency on the pressure and thus - as expected - a smaller degree of deformability compared to the former. This behaviour is in a good agreement with the results shown in Figure 8.7. The droplets that contain the active bacteria and that are in water appear to be more deformable, thus softer than the rest of the samples.

According to Figure 8.7, *Pseudomonas atlantica*-containing droplets in oil have an effective size that is 78-83% of their size prior to the DLD experiments. Thus their effective size, that also determines their displacement in the device, lies within the range of 6.7-7.3 μm. Similarly, the R/R_{eff} ratio for *Pseudomonas atlantica*-containing droplets in water varies from 1.19 to 1.48 resulting in effective sizes in the range of 6-7.5 μm. Finally, *Bacillus subtilis*-containing droplets in water have an R/R_{eff} ratio from 1.19 to 1.28 and depending on the applied pressure, their effective diameters vary from 6.6 μm to 7.2 μm.

By comparing the measured absolute effective sizes of the droplets from the recorded videos with the sizes that correspond to their distribution at the exit of the device (given by the theoretical D_c values in Figure 8.13), it appears that the droplet samples which were run in water are sorted in the DLD as if they would be smaller than expected (see Figure 8.14). Specifically, *Pseudomonas atlantica*-containing droplets in water behave as particles that are 3-4 μm smaller and *Bacillus subtilis*-containing droplets in water appear to be 2-3 μm smaller. On the contrary *Pseudomonas atlantica*-containing droplets in oil appear to be approximately 6 μm in diameter which is close to the expected size. As previously mentioned, in the case of the samples in water, free bacteria were observed in the solution after escaping the droplets. The bacteria, with dimensions of $0.5 \times 0.5 \times 3$ μm^3, flow in a "zig zag" motion

and exit the DLD device at the first post gaps (Figure 8.15). The presence of the bacteria as well as small debris in the solution results in a shift of the mean displacements of the droplets towards smaller values, by 100-200 μm approximately. In addition, a slight clogging by droplets that were stuck at the entrance of the device in the case of the samples in water, might have also resulted in shifted distributions. However there could be other unknown explanations why there is this difference between the directly measured effective size of the droplets and the theoretically expected critical size. The high standard deviations for the mean displacements of the samples in oil and the *Bacillus subtilis*-containing droplets in water indicate the heterogeneity in their effective sizes.

For the droplet samples run in oil, the displacement of approximately 5000 droplets was examined at high pressures and of approximately 500 droplets at lower pressures. It is important to mention however that for the droplet samples which were run in water, much less droplets were examined. This was due to the fact that the latter were diluted during the extraction from the oil. In addition due to the low contrast of these samples, many droplets were omitted by the software during the video analysis, as they were mistaken for noise.

References

Ng, K. W., Kugler, L. E., Doty, S. B., Ateshian, G. A., and Hung, C. T. (2009), Scaffold degradation elevates the collagen content and dynamic compressive modulus in engineered articular cartilage, *Osteoarthritis and Cartilage* 17 (2), pp. 220–227, DOI: 10.1016/j.joca.2008.06.013.

Shoichet, M. S., Li, R. H., White, M. L., and Winn, S. R. (1996), Stability of Hydrogels Used in Cell Encapsulation: An In Vitro Comparison of Alginate and Agarose, *Biotechnology and Bioengineering* 50 (4), pp. 374–381, DOI: 10.1002/(SICI)1097-0290(19960520)50:4<374::AID-BIT4>3.0.CO;2-I.

Stolz, M., Raiteri, R., Daniels, A. U., VanLandingham, M. R., Baschong, W., and Aebi, U. (2004), Dynamic Elastic Modulus of Porcine Articular Cartilage Determined at Two Different Levels of Tissue Organization by Indentation-Type Atomic Force Microscopy, *Biophysical Journal* 86 (5), pp. 3269–3283, DOI: 10.1016/S0006-3495(04)74375-1.

9 Conclusions

In the current project a new method for monitoring the cellular secretion was presented. Agarose gel microdroplets were used as biosensors for β-agarase enzymes, that are secreted from *Pseudomonas atlantica* bacteria.

Pseudomonas atlantica bacteria were initially encapsulated in agarose droplets using a droplet-based microfluidic device. A DLD device was then used to detect the presence of the enzymes by examining the deformability of the droplets as a function of the applied flow pressure. As a negative control, non-secreting bacteria *Bacillus subtilis* as well as polystyrene beads were encapsulated and tested in the DLD device. In addition, the bacteria-containing droplets were tested in the DLD using oil instead of water as a medium, and the differences in their deformability were examined.

The results showed that at high shear rates *Pseudomonas atlantica*-containing droplets that were run in water tended to deform more than the droplets that were run in oil, the *Bacillus subtilis*-containing samples, as well as the droplets that contained the polystyrene beads. At lower pressures however all samples exhibited a similar degree of deformation. This behaviour can be explained by the fact that in the *Pseudomonas atlanctica*-containing droplets, the secreted β-agarase hydrolyzes the agarose gel, thus results in the softening of the droplets. When run in the DLD, the soft droplets exhibit a high degree of deformation. On the contrary, no enzymes are present in the droplets that do not contain the secreting bacteria. This results in more rigid droplets, which exhibit a smaller degree of deformation even at high shear rates.

Even though the results show a tendency of the droplets that contained the secreting bacteria to behave as expected, more experiments in the future as

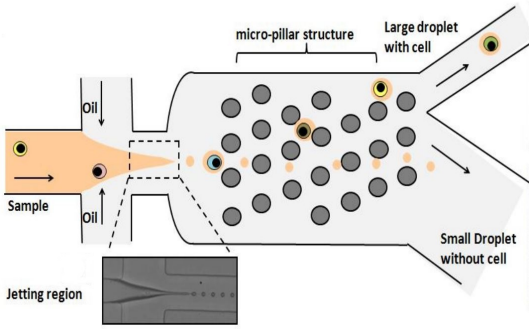

Figure 9.1: A droplet-based flow-focusing device where the deterministic lateral displacement geometry is used for a high-throughput encapsulation.[1]

well as positive controls would be necessary to verify the results and validate the method.

9.1 Outlook

One of the additional experiments that could be performed in the future is the examination of the behaviour of agarose droplets in the presence of pure β-agarase enzymes. In addition, different cellular types could be used as model systems for the investigation of secretion using the presented method. For cells that are big enough to influence the size of the generated droplets when encapsulated, a droplet-based microfluidic device similar to the one described by Jing *et al.* (2013) could also be used (Figure 9.1). In this device, droplets that contain cells are sorted from empty droplets during their synthesis, by using the deterministic lateral displacement technique, resulting in a high throughput encapsulation. For a higher throughput sorting of the particles based on their deformability, a DLD device with a smaller range of critical diameters and a smaller increase step could be designed.

In the future, the current method could also be used for the detection of different cellular signals, like changes in the pH, using the appropriate biocompatible hydrogels. For instance, hydrogel droplets that respond to changes of the environmental pH by swelling or shrinking could be also sorted using the DLD method based on their size. These types of signals are harder to assay using optical methods since the use of non-biocompatible chemicals

[1] Adapted from Jing *et al.* (2013) with permission from The Chemical and Biological Microsystems Society.

might be required. Finally by using hydrogels into the polymeric network of which antigens and their specific antibodies are cross-linked, antigen (or antibody) sensitive hydrogels can be created (Miyata *et al.*, 1999a; Miyata *et al.*, 1999b). In the presence of secreted free antigens in the solution for instance, the antibody-antigen cross-links dissociate and the antibodies in the gel network bind to the free antigens. This results in a swelling of the hydrogel, that could also be detected with the method presented herein.

This method can be thus extended in several different systems, indicating that it could be the precursor for future experiments that could yield interesting results. There is a great potential for it to constitute a strong tool for the investigation of the single-cell behaviour and the cellular heterogeneity in secretion for pharmaceutical and biotechnological applications.

References

Jing, T., Ramji, R., Warkiani, M. E., Lim, C. T., Han, J., and Chen, C. H. (2013), High Throughput Single Cancer Cell Encapsulation and Self Sorting for Protease Assay by Using Jetting Microfluidics, *17th International Conference on Miniaturized Systems for Chemistry and Life Sciences*, 27-31 October 2013, Freiburg, Germany, pp. 1373–1375.

Miyata, T., Asami, N., and Uragami, T. (1999a), A reversibly antigen-responsive hydrogel, *Nature* 399, pp. 766–769, DOI: 10.1038/21619.

— (1999b), Preparation of an Antigen-Sensitive Hydrogel Using Antigen-Antibody Bindings, *Macromolecules* 32 (6), pp. 2082–2084, DOI: 10.1021/ma981659g.

Self Reflection

In this project I was given the opportunity to work and obtain hands-on experience on the field of microfluidics and their applications in biophysics, that I always found very interesting. Working on this project however was also challenging, as several times I encountered obstacles that I had to overcome. Many different parameters had to be taken into consideration in order to perform a successful experiment. Since biological samples were used in the experiments, taking the most suitable approach and preparing the experimental set-up was very crucial. A good time management as well as maintaining my focus on the goal and finding appropriate solutions to the problems that might have appeared, were some of the skills I developed during my work. Finally, the performed literature research helped me gain insight into the field, understand how an experiment can be approached and which are its important aspects.

A DLD device characteristics

Table A.1: Characteristics of the DLD device. The center-to-center post distance λ is 32 μm and the post gap d is 12 μm.

Section	**$\Delta\lambda$(μm)**	**N**	**Rows**	**D_c(μm)**	**Displacement (μm)**
1	0.8	36.71	200	2.86	160
2	1.2	26.67	130	3.47	316
3	1.6	20.00	100	3.99	476
4	2	16.00	80	4.44	636
5	2.6	12.31	60	5.04	792
6	3.2	10.00	50	5.56	952
7	3.8	8.42	40	6.04	1104
8	4.4	7.27	35	6.48	1258
9	5.2	6.15	30	7.02	1414
10	6.0	5.33	25	7.53	1564
11	6.8	4.71	20	7.99	1700
12	7.8	4.10	20	8.53	1856
13	8.8	3.64	15	9.04	1988

B Soft Lithography

1. Preparation of PDMS device:

    - Mix 10 g PDMS and 1 g hardener using a pipette tip for 3 minutes.
    - De-gas the mixture in a vacuum chamber for 1 hour.
    - Pour the PDMS mixture on a patterned silicon wafer and incubate in the oven at 80 ℃ for 1 hour.
    - Pour the PDMS mixture on a glass slide and spin-coat it at 800 rpm, in order to create a thin layer of PDMS on the slide. Incubate the glass slide in the oven at 80 ℃ for 1 hour.
    - Remove the PDMS device from the wafer and transfer it to a clean 50 mm x 75 mm glass slide.
    - Cut the PDMS layer to fit on the glass slide and punch holes in the inlets and outlets of the device.

2. Oxygen plasma treatment:

    - Tip the PDMS device over on the glass slide (channels facing upwards) and insert it in the oxygen plasma treatment microwave.
    - Insert the PDMS-coated glass slide in the oxygen plasma treatment microwave.
    - Turn microwave power and valves on.
    - Turn vacuum pump on until the pressure is 0.8 mbar.
    - Turn on O_2, set pressure to 8 mbar and wait for 60 seconds.
    - Microwave the sample, maximum effect for 30 seconds. Turn O_2 off.

- Turn on N_2, set pressure to 10 mbar and wait for 60 seconde. Turn N_2 off.
- Set vacuum pump to ventilation. When atmospheric pressure is reached, retrieve samples.
- Turn microwave valves and power off.

3. Finalization of device:

   - Place the PDMS device on the treated PDMS-coated glass slide, with channels facing downwards.
   - Add 5 μL PLL-g-PEG in the inlets (Hydrophilic devices).
   - Glue 5 mm x 3 mm in diameter reservoir tubes on top of the inlets and outlets of the device.
   - Wait 1 hour for the glue to dry.

4. Surface Silanization (Hydrophobic devices):

   - Evacuate and refill the loading chamber to flush away remaining gases. Repeat three times.
   - Load the PDMS devices.
   - Repeat the flushing of the loading chamber.
   - Insert the devices into the glove box.
   - Place the devices into a petri dish and cover with the lid.
   - Add 75 μL of the anti-sticking reagent ([Tridecafluoro - 1, 1, 2, 2 - tetrahydrooctyl]trichlorosilane) into the petri dish using a needle.
   - Wash needle in n-Hexane AnalaR NORMAPUR®.
   - Bake the petri dish on a hot plate at 150 ℃ for 24 hours.
   - Remove devices from the petri dish.
   - Evacuate and refill the loading chamber. Repeat three times.
   - Take the PDMS devices out of the glove box.

C Beta-agarase hydrolysis assay

Preparation of the agarase solution:

Dilution of pure β-agarase in PBS at two different concentrations: 10 units/mL and 50 units/mL.

Hydrolysis assay with an incubation step:

1. For the preparation of 1% ULMP agarose, 0.03 g of ULMP agarose are mixed with 3 mL of LB growth medium and microwaved for 30 seconds
2. 0.5 mL of agarose solution is placed in an eppendorf tube and allowed to harden at room temperature for 30 minutes (or in an ice bath for 15 minutes)
3. To the hardened agarose 100 μL of the β-agarase solution are added
4. Incubation of the eppendorf tube in a water bath at 37 ℃ - 40 ℃ for 1 hour.
5. The eppendorf tube is removed from the water bath and cooled in an ice bath for 15-20 minutes.
6. Inspection for liquefaction of the agarose gel

Hydrolysis assay without an incubation step:

1. For the preparation of 1% ULMP agarose, 0.03 g of ULMP agarose are mixed with 3 mL of LB growth medium and microwaved for 30 seconds
2. 0.5 mL of agarose solution is placed in an eppendorf tube and allowed to harden at room temperature for 30 minutes (or in an ice bath for 15 minutes)
3. To the hardened agarose 50 μL of the β-agarase solution are injected with a needle

4. The eppendorf tube is kept at room temperature for 2-3 hours.
5. It is then cooled in an ice bath for 15-20 minutes.
6. Inspection for liquefaction of the agarose gel

D *Bacillus subtilis* growth protocol

1. Preparation of the agar plates:

   - Mix 33 g of Tryptose Blood Agar Base with 1 L milliQ water.
   - Add 500 mL of the solution in each of two flasks
   - Autoclave the flasks at 121 ℃ for 2.5 - 3 hours.
   - Cool one agar- containing flask to 50 ℃ for 20 minutes.
   - Fill in 20 culture plates with the agar solution.
   - Wait 1 hour for the agar to solidify in the plates.

2. Preparation of the LB growth medium:

   - Mix 25 g of LB with 1 L milliQ water.
   - Add 50 mL of the solution in each of 10 small flasks and 500 mL of the solution in a larger flask.

3. Cultivation of *Bacillus subtilis* bacteria:

   - With a loop and in a zig-zag motion place the *Bacillus subtilis* bacteria (from the frozen stock) onto the agar plates.
   - Incubate the plates overnight at 37 ℃.
   - Extract a few bacterial colonies that were grown onto the agar plates and inoculate 10 mL of the LB medium in a conical flask.
   - Incubate the conical flask at 37 ℃ (mixing at 200 rpm) for 4-5 hours.
   - The final sample has a concentration of 10^6 cells/mL.

E Preparation of *Pseudomonas atlantica* bacteria for Scanning Electron Microscopy

1. Bacterial cell fixation

   - Wash cells twice in phosphate-buffered saline (PBS).
   - Fixate the cells in an ethanol/acetic acid solution (3:1) for 10 minutes.
   - Wash cells twice in PBS.
   - Successively suspend the cells in different concentrations of ethanol (25%, 50%, 75%, 95%, 99,7%). Wait 5 minutes at each step.
   - Drip 100 μL of the bacterial solution onto an adhesive Polysine™glass slide.
   - Air-dry overnight.

2. Sputter coating with platinum of air-dried bacterial sample.